

Learning the Exact Time Integration Algorithm for Initial Value Problems by Randomized Neural Networks

Suchuan Dong*, Naxian Ni
 Center for Computational and Applied Mathematics
 Department of Mathematics
 Purdue University, USA

(February 15, 2025)

Abstract

We present a method leveraging extreme learning machine (ELM) type randomized neural networks (NNs) for learning the exact time integration algorithm for initial value problems. The exact time integration algorithm for non-autonomous (including autonomous) systems can be represented by an algorithmic function in higher dimensions, which satisfies an associated system of partial differential equations with corresponding boundary conditions. Our method learns the algorithmic function by solving this associated system using ELM with a physics informed approach. The trained ELM network serves as the learned algorithm and can be used to solve the initial value problem with arbitrary initial data or arbitrary step sizes from some domain. When the right hand side of the non-autonomous system exhibits a periodicity with respect to any of its arguments, while the solution itself to the problem is not periodic, we show that in this case the algorithmic function is either periodic, or when it is not, satisfies a well-defined relation for different periods. This property can greatly simplify the network training for algorithm learning in many problems. We consider explicit and implicit NN formulations, leading to explicit and implicit time integration algorithms, and discuss how to train the ELM network by the nonlinear least squares method. Extensive numerical experiments with benchmark problems, including non-stiff, stiff and chaotic systems, show that the learned NN algorithm produces highly accurate solutions in long-time simulations, with its time-marching errors decreasing nearly exponentially with increasing degrees of freedom in the neural network. We compare extensively the computational performance (time-marching accuracy vs. time-marching cost) between the current NN algorithm and the leading traditional time integration algorithms. The learned NN algorithm is computationally competitive, markedly outperforming the traditional algorithms in many problems.

Keywords: *extreme learning machine, randomized neural network, scientific machine learning, nonlinear least squares, exact time integration, exact flow map*

1 Introduction

This work concerns the development of accurate and efficient methods for solving initial value problems (IVPs), by learning their exact time integration algorithm with artificial neural networks. Initial value problems with systems of ordinary differential equations (ODEs) are ubiquitous in modeling natural phenomena and engineered systems. Problems as diverse as population dynamics, the spread of diseases, chemical reactions, celestial mechanics, dynamical systems, biological pattern formation, and the economic markets can be modeled by such systems. They also arise, upon spatial discretization, from time-dependent partial differential equations (PDEs) describing the evolution of physical systems based on first principles such as the conservation laws and thermodynamic principles [15, 36, 17, 18, 78]. The models arising from practical applications are usually nonlinear and can rarely be solved by analytical methods. Numerical simulations are therefore of fundamental importance and play a critical role in understanding the dynamics of these systems.

*Author of correspondence. Email: sdong@purdue.edu

Time marching algorithms for IVPs are traditionally based on Taylor series expansions. Research in the past decades has led to accurate and robust methods with provable convergence based on this approach [8, 37, 38], which have become the cornerstone in computational science and engineering.

The emergence of artificial neural networks [35] and their application in scientific computing, a.k.a. scientific machine learning (SciML) [45, 66, 70, 27, 73, 21, 48, 23, 74, 61, 62], in recent years have stimulated promising new approaches for simulating dynamical systems [64, 66, 70, 44, 53, 75, 31, 16, 57]. NN-based methods for such problems can be broadly classified into two types, as pointed out in [49], direct solution models and time-stepper models. Direct solution models seek the solution to the IVP directly, in which the network input denotes the independent variable and the output represents the solution. Representative techniques in this category include the physics-informed neural network (PINN) method [66], deep Galerkin method (DGM) [70], and their many extensions and variants; see [45, 14] for a review of related techniques. Because the trained NN corresponds to a specific input or initial condition, the direct solution model needs to be re-trained if the initial data changes. The time-stepper models, on the other hand, follow an approach analogous to traditional numerical solvers. Given the current state of the system, the model attempts to compute the state at some point in the future. Accordingly, the NNs for time-stepper models are generally auto-regressive in nature, aiming to capture the dynamics of the system. The trained time-stepper model can handle different initial data or input, without the need for re-training. Early works on time-stepper models have focused on the data-driven modeling of dynamical systems, in which the governing equations are unknown and are approximated by the solution trajectory data [64, 63, 12]. A residual network (ResNet) structure and stacked ResNets with a recurrent or recursive configuration are proposed in [64] to approximate the unknown governing equations and learn a discrete flow map of the autonomous systems. This technique is extended to non-autonomous systems in [63], where the non-autonomous term is expanded in terms of a local set of bases, and to cases with partially observed state variables [12]; see recent related works in [10, 55]. A hierarchical time-stepper based on deep neural networks (DNN) is developed in [53] to approximate the system flow map over a range of time scales, in which multiple DNNs are trained corresponding to a number of step sizes using the trajectory data; see [39] for an adaptive time-stepping scheme with the hierarchical time-stepper. In [16] deep reinforcement learning has been combined with classical numerical solvers to determine the step sizes in adaptive time-stepping. In [79] NN structures are designed to satisfy the symmetric degeneracy conditions in the GENERIC formalism for simulating dynamical systems, and their universal approximation property has been established. We also refer the reader to [11, 47, 33] (among others) for neural ODEs and to [49] for a survey of other related techniques.

Given a non-autonomous system of ODEs, we seek the exact time integration algorithm for this system. An exact time integration (or time marching) algorithm refers to a discrete scheme that can produce numerical solutions matching exactly the true solutions to the system for all step sizes within a range; see Section 2 for its definition. This type of algorithms is also known as the exact finite difference schemes or non-standard finite difference (NSFD) schemes [56]. The exact finite difference schemes for a number of problems have been constructed explicitly in [56], by using denominator functions for approximating discrete derivatives and by special treatments of the nonlinear terms involved in the equations. However, constructing the exact discrete scheme for an arbitrary given system of differential equations is virtually impossible, unfortunately, because otherwise this will be tantamount to knowing the general forms of the solution to the given system [56].

This motivates the current work for learning the exact time integration algorithms through artificial neural networks, by leveraging the NN’s universal approximation power for function approximation. Viewed from the dynamical systems perspective, the exact time integration algorithm is closely related to the exact flow map (or evolution semigroup) [71] of the system. Given a system of differential equations, suppose the system has a unique solution for any given initial condition. Then the exact time integration algorithm exists, and we would like to learn this algorithm from the given system. The learned algorithm then provides a method for solving this system, under any given initial condition or step size. The problem considered here is different from the so-called flow-map learning in previous studies (see e.g. [64, 13, 53], among others), where the governing differential equations are unknown and a time-stepper model is learned based on the solution trajectory data obtained from either measurements or external numerical solvers. In contrast, for the problems considered in this paper, the system of differential equations is given and we seek the exact time integration algorithm for this system. No other data about the system is available, and our method does not rely on any external numerical solver.

Given a system of non-autonomous (including autonomous) ODEs, the exact time integration algorithm

for this system can be represented by a vector-valued function in higher dimensions, which in the current paper will be referred to as the algorithmic function of the given system. The algorithmic function satisfies an associated system of partial differential equations, together with corresponding boundary conditions. We learn the exact time integration algorithm by solving the associated system of PDEs for the algorithmic function with a physics informed approach, leveraging a type of randomized feedforward neural networks often known as extreme learning machines (ELMs) [19, 24, 76].

Randomized NNs (or random-weight NNs) are neural networks with a subset of the network parameters assigned to random values and fixed (non-trainable) while only the rest of the network parameters are trained. A simple strategy underlies randomized NNs. Since optimizing the entire set of NN parameters is extremely difficult and costly, randomized NN attempts to randomly assign and fix a portion of the network parameters, so that the ensuing network training problem can become simpler, without severely compromising the network’s achievable approximation capability [24, 58]. ELM is a particular type of randomized feedforward NNs, in which all the hidden-layer parameters are assigned to random values and fixed (non-trainable) while only the output-layer parameters are trained. ELM was originally proposed in [41] for linear classification and regression problems, but has since found widespread applications in many areas [1]. A close cousin to ELM is the random vector functional link (RVFL) networks [60]. ELM type randomized NNs, with a single hidden layer, are known to be universal function approximators [43, 42, 34].

The use of ELM type randomized NNs for scientific computing, particularly for solving partial differential equations, occurs quite recently and has flourished in the past few years [19, 68, 7, 76]. We refer the reader to [59, 26, 19, 52, 7, 9, 50, 65, 6, 72] (among others) for ELM type methods for linear PDEs, to [19, 20, 68, 28, 24, 58, 22, 76] (among others) for nonlinear PDEs, and to a recent work [30] for neural operators. Many studies (including those from our group) have shown that ELM can produce highly accurate solutions to linear and nonlinear PDEs, exhibiting spectral-like accuracy [19, 58], with a competitive computational cost [24]. The ELM errors decrease exponentially with increasing number of degrees of freedom for smooth solutions, and can reach the level near machine accuracy as the degrees of freedom become large [24]. Several studies have looked into the computation of ODEs based on randomized NNs [77, 51, 59, 19, 67, 29, 32]. These studies stem from the direct solution model, in which the NN learns the solution corresponding to a specific initial condition. As a result, with different initial data, the NN has to be re-trained. In contrast, with the method herein, the trained NN can solve the problem with arbitrary initial data from some domain, with no need for re-training. This is a major difference between these studies and the current work.

In this paper we present a method based on ELM-type randomized NNs for learning the exact time integration algorithm of non-autonomous and autonomous systems. Our method learns the algorithmic function using ELM by solving its associated system of partial differential equations with a physics informed approach. We explicitly incorporate an approximation of the solution field into the NN formulation, so that the ELM network effectively learns the corresponding error function. We consider explicit and implicit NN formulations and discuss how to train the ELM network by the nonlinear least squares (Gauss-Newton) method. Accordingly, the trained NN gives rise to explicit or implicit time integration algorithms for solving the system. In particular, we investigate the effect on the algorithm learning when the right hand side (RHS) of the non-autonomous system exhibits a periodicity with respect to time or to any component of the solution variable. We show that in this case, while the solution itself to the IVP is not periodic, the algorithmic function is either periodic, or when it is not, shows a well-defined relation for different periods. This means that, whenever the RHS of the non-autonomous system exhibits a periodicity with respect to any of its arguments, the NN only needs to be trained on a domain covering one period along the corresponding directions, and the trained NN can be used to solve the problem on arbitrarily long time horizons (in case of temporal periodicity of RHS) or for those corresponding solution components taking arbitrary values on the real axis. These properties can greatly simplify the network training and algorithm learning for many problems. In addition, we find that it is often crucial to incorporate domain decomposition into the algorithm learning, especially for stiff problems. In this case, a local ELM-type randomized NN learns the algorithmic function on each sub-domain, and the local NNs collectively represent the algorithmic function over the entire training domain. What is most attractive lies in that different local NNs are not coupled, due to the nature of the PDE system for the algorithmic function, and thus they can be trained completely separately.

We present extensive numerical experiments with several benchmark problems (including non-stiff, stiff, and chaotic systems) to evaluate the performance of the learned NN algorithm. We show that the learned algorithm produces highly accurate solutions in long-time simulations. Its time-marching errors decrease nearly

exponentially as the number of degrees of freedom (training collocation points, or training parameters) in the NN increases, while its time-marching cost grows only quasi-linearly. We compare extensively the computational performance (time-marching accuracy vs. time-marching cost) between the current NN algorithm and the leading traditional time integration algorithms (with adaptive time-stepping and adaptive-order), including DOP853 (Dormand Prince, order 8) [37], RK45 (explicit Runge-Kutta, order 5) [25], and Radau (implicit Runge-Kutta Radau IIA, order 5) [38], among others. The learned NN algorithm is computationally very competitive, markedly outperforming the traditional algorithms in almost all problems.

The contributions of this paper lie in three aspects: (i) the ELM-based method for learning the exact time integration algorithms and the learned NN algorithms for accurately and efficiently solving non-autonomous and autonomous systems; (ii) the illumination of properties of the algorithmic function when the RHS of non-autonomous (including autonomous) systems exhibits a periodicity with respect to any of its arguments, which can be used to greatly simplify the network training and algorithm learning; and (iii) the comparison with traditional time integration algorithms and demonstration of the competitive and superior computational performance of the learned NN algorithms.

The method presented here has been implemented in Python using the Tensorflow and Keras libraries. The numerical tests are performed on a MAC computer (3.2GHz Quad-Core Intel Core i5 processor, 24GB memory) in the authors' institution.

The rest of this paper is organized as follows. In Section 2 we discuss the properties of the algorithmic function, its representation by ELM-type randomized NNs, the network training by the nonlinear least squares method, and how to use the learned algorithm to solve non-autonomous and autonomous systems. Section 3 consists of a comprehensive set of numerical tests to assess the performance of the presented method with several benchmark problems. We compare extensively the learned NN algorithms with leading traditional time integration algorithms. Section 4 provides further comments on several aspects of the current method to conclude the presentation. The appendix includes proofs of several theorems from Section 2 concerning the properties of the algorithmic function.

2 Learning the Exact Time Integration Algorithm

2.1 Exact Time Marching Scheme

Let n be a positive integer, and we consider the initial value problem on $t \in (a, b)$,

$$\frac{dy}{dt} = f(y, t), \tag{1a}$$

$$y(t_0) = y_0, \tag{1b}$$

where t denotes the time, $t_0 \in (a, b)$ is the initial time, $y : (a, b) \subset \mathbb{R} \rightarrow \mathbb{R}^n$ denotes the solution, $f : \mathbb{R}^n \times \mathbb{R} \rightarrow \mathbb{R}^n$ is a prescribed function, and $y_0 \in \mathbb{R}^n$ denotes the initial data.

To numerically solve this system, a time integration algorithm produces a sequence $\{y_k \in \mathbb{R}^n \mid \text{integer } k \geq 0\}$ as approximations to the solution $y(t)$ at discrete instants, $\{y(t_k) \mid t_k = t_0 + kh, k \geq 0\}$, where h denotes the step size. Interestingly, there exist discrete schemes that can produce exact results to the system (1). The forms of such schemes for several problems have been explicitly constructed in [56]. Following [56], we define an exact time integration (or time marching) algorithm as follows,

Definition 2.1. A time marching algorithm is said to be exact if it produces results identical to the exact solution for arbitrary values of $h \in (0, h_{\max}]$ ($h_{\max} > 0$ denoting some constant), i.e. $y_k = y(t_k)$ for $k \geq 0$.

Suppose $f(y, t)$ is continuous and satisfies the Lipschitz condition $\|f(y, t) - f(z, t)\| \leq \lambda \|y - z\|$ for some constant λ . Then the system (1) has a unique solution within a neighborhood of t_0 [37]. We re-write this solution as,

$$y(t) = \psi(y_0, t_0, t), \quad t \in [t_0 - \delta, t_0 + \delta] \tag{2}$$

for some $\delta > 0$, where $\psi(y_0, t_0, t_0) = y_0$ and the dependence of the solution on y_0 and t_0 has been made explicit. The existence of the exact time marching scheme for (1) is established in [71, 56], given by the following result (see pages 61-62 of [56]).

Theorem 2.1. ([56]) *The system (1) has an exact time integration scheme given by*

$$y_{k+1} = \psi(y_k, t_k, t_k + h), \quad k \geq 0, \quad (3)$$

where ψ is given in (2) and h is the step size.

This result indicates that by acquiring the function $\psi(y_0, t_0, t)$, for $y_0 \in \Omega \subset \mathbb{R}^n$, $t_0 \in (a, b) \subset \mathbb{R}$ and $t \in [t_0 - \delta, t_0 + \delta]$, one can attain the exact time integration algorithm (3) for solving (1). In the dynamical systems parlance, this function is often referred to as the evolution map (or flow map, evolution semigroup) [71]. This is a high-dimensional vector-valued function, and is unknown for an arbitrary given $f(y, t)$. Attaining ψ is in general even more challenging than solving the original system (1). In the current work we use randomized NNs to learn the function $\psi(y_0, t_0, t)$, and the trained network provides an approximation to the exact time integration algorithm. The trained NN can be used as a time marching algorithm for solving (1), with arbitrary initial data $(y_0, t_0) \in \Omega \times (a, b)$ and arbitrary step size $h \in (0, h_{\max}]$. It is crucial to note that it is only necessary to learn $\psi(y_0, t_0, t)$ for t within a neighborhood of t_0 .

Specifically, we will learn the function $\psi(y_0, t_0, t)$ by ELM-type randomized neural networks [19, 24, 58, 76], leveraging ELM's universal approximation capability [43, 42], high accuracy, faster training, and effectiveness for function approximation in high dimensions [19, 76]. It is necessary to distinguish non-autonomous and autonomous systems when learning the exact time integration algorithm. We will first discuss general non-autonomous systems, and then restrict our attention to autonomous systems.

2.2 Learning Exact Time Marching Algorithm for Non-Autonomous Systems

Let us consider the general non-autonomous system (1) and discuss how to learn the function ψ by ELM. Since it is only necessary to learn ψ for t within some neighborhood of t_0 , we define

$$\xi = t - t_0, \quad y(t) = y(t_0 + \xi) = Y(\xi), \quad (4)$$

where $y(t)$ is the solution to (1). The system (1) can be reformulated in terms of $Y(\xi)$ into,

$$\frac{dY}{d\xi} = f(Y, t_0 + \xi), \quad (5a)$$

$$Y(0) = y_0. \quad (5b)$$

Since the solution to system (5) depends on y_0 , t_0 and ξ , we re-write it as

$$Y(\xi) = \psi(y_0, t_0, \xi), \quad (6)$$

where $\psi : \mathbb{R}^n \times \mathbb{R} \times \mathbb{R} \rightarrow \mathbb{R}^n$ is the function we are pursuing here and provides the exact time marching algorithm. Henceforth we will refer to $\psi(y_0, t_0, \xi)$ as the algorithmic function for system (1).

In light of (5), the algorithmic function $\psi(y_0, t_0, \xi)$ is determined by the following partial differential equations,

$$\frac{\partial \psi}{\partial \xi} = f(\psi(y_0, t_0, \xi), t_0 + \xi), \quad (7a)$$

$$\psi(y_0, t_0, 0) = y_0. \quad (7b)$$

Our objective is to determine the function $\psi(y_0, t_0, \xi)$, for $y_0 \in \Omega \subset \mathbb{R}^n$, $t_0 \in [T_0, T_f] \subset \mathbb{R}$, and $\xi \in [0, h_{\max}] \subset \mathbb{R}$ with prescribed Ω , T_0 , T_f and h_{\max} , such that the system (7) is satisfied. $\psi(y_0, t_0, \xi)$ is an n -vector valued function of $(n + 2)$ variables, where n denotes the dimension of system (1).

2.2.1 Property of Algorithmic Function $\psi(y_0, t_0, \xi)$ When $f(y, t)$ Exhibits Some Periodicity

We next discuss a useful property of the algorithmic function $\psi(y_0, t_0, \xi)$ when the RHS of (1a), $f(y, t)$, exhibits a periodicity with respect to t or to some components of y . This property can be used to simplify the NN training for learning $\psi(y_0, t_0, \xi)$ when applicable. In this subsection we assume that $(y, t) \in \mathbb{R}^n \times \mathbb{R}$ in problem (1) and $\xi \in [0, h_{\max}]$ for a prescribed constant $h_{\max} > 0$. We further make the following assumption:

Assumption 2.1. The function $f(y, t)$, with $(y, t) \in \mathbb{R}^n \times \mathbb{R}$, is such that the problem (1) has a unique solution for all $t \in \mathbb{R}$, with arbitrary $(y_0, t_0) \in \mathbb{R}^n \times \mathbb{R}$.

This assumption can be satisfied, e.g. if $f(y, t)$ is globally Lipschitz on $\mathbb{R}^n \times \mathbb{R}$ (see Theorem 2.1.3 in [71]). Under this assumption, it can be noted that problem (7) has a unique solution $\psi(y_0, t_0, \xi)$ for all $(y_0, t_0, \xi) \in \mathbb{R}^n \times \mathbb{R} \times [0, h_{\max}]$.

We look into the effect on $\psi(y_0, t_0, \xi)$ if $f(y, t)$ exhibits some periodicity, and consider the following two cases. In the first case, $f(y, t)$ is periodic with respect to t , i.e.

$$f(y, t + T) = f(y, t), \quad \text{for all } (y, t) \in \mathbb{R}^n \times \mathbb{R}, \quad (8)$$

where $T > 0$ is the fundamental period. In the second case, $f(y, t) = f(y_1, y_2, \dots, y_n, t)$ is periodic with respect to y_i with the fundamental period $L_i > 0$, for some $1 \leq i \leq n$, i.e.

$$f(y + L_i \mathbf{e}_i, t) = f(y, t), \quad \text{for all } (y, t) \in \mathbb{R}^n \times \mathbb{R}, \quad (9)$$

where $\mathbf{e}_k = (0, \dots, 0, 1, 0, \dots, 0) \in \mathbb{R}^n$ ($1 \leq k \leq n$) denote the standard basis vectors of \mathbb{R}^n .

If $f(y, t)$ is periodic in t , the solution $y(t)$ to the initial value problem (1) may or may not be a periodic function. It depends on $y(t)$ for $t \in [t_0, t_0 + T]$, where T is the period of $f(y, t)$ and t_0 is the initial time. The following lemma summarizes the result.

Lemma 2.2. *Suppose $f(y, t)$ is periodic in t with the period T and $y(t)$ denotes the solution to problem (1). If $y(t_0 + T) = y(t_0)$, then $y(t)$ is periodic with a period T under the Assumption 2.1, i.e. $y(t + T) = y(t)$ for all $t \in \mathbb{R}$.*

A proof of this result is provided in the Appendix. For a general periodic $f(y, t)$ with the period T , when restricted to $t \in [t_0, t_0 + T]$, the solution $y(t)$ to (1) in general does not satisfy $y(t_0 + T) = y(t_0)$, unless $\int_{t_0}^{t_0+T} f(y(t), t) dt = 0$. This lemma therefore indicates that the solution to problem (1) in general is not a periodic function, even though $f(y, t)$ is periodic in t .

The algorithmic function $\psi(y_0, t_0, \xi)$, on the other hand, would be periodic with respect to t_0 , if $f(y, t)$ is periodic in t . This result is summarized in the following theorem.

Theorem 2.3. *Suppose $f(y, t)$ is periodic in t with the period T . Then $\psi(y_0, t_0, \xi)$ from the system (7) is periodic in t_0 with a period T under the Assumption 2.1, i.e. $\psi(y_0, t_0 + T, \xi) = \psi(y_0, t_0, \xi)$ for all $(y_0, t_0, \xi) \in \mathbb{R}^n \times \mathbb{R} \times [0, h_{\max}]$.*

A proof of this theorem is provided in the Appendix. This result suggests that, if $f(y, t)$ is periodic in t , we only need to learn the algorithmic function $\psi(y_0, t_0, \xi)$ over one period along the t_0 direction for non-autonomous systems. The learned algorithm can then be used to compute the solution $y(t)$ to problem (1) for all $t \in \mathbb{R}$ (i.e. arbitrarily long time horizons), which, as noted above, is not periodic in general.

If $f(y, t)$ is periodic with respect to a component of y , the algorithmic function $\psi(y_0, t_0, \xi)$ is not periodic with respect to the corresponding component of y_0 . Instead, along the direction of that component, ψ satisfies a well-defined relation as given below.

Theorem 2.4. *Suppose $f(y, t)$ is periodic in y_i with the period L_i (see (9)), for some $1 \leq i \leq n$. Then $\psi(y_0, t_0, \xi)$ from system (7) satisfies the following relation under the Assumption 2.1,*

$$\psi(y_0 + L_i \mathbf{e}_i, t_0, \xi) = \psi(y_0, t_0, \xi) + L_i \mathbf{e}_i, \quad \text{for all } (y_0, t_0, \xi) \in \mathbb{R}^n \times \mathbb{R} \times [0, h_{\max}]. \quad (10)$$

A proof of this theorem is provided in the Appendix. This result suggests that, if $f(y, t)$ is periodic with respect to some components of y , we only need to learn $\psi(y_0, t_0, \xi)$ over one period for the values of those corresponding components of y_0 . The learned algorithm can then be used to compute the solution $y(t)$ to problem (1), in which those components of $y(t)$ corresponding to the periodic directions of $f(y, t)$ can each take arbitrary values on \mathbb{R} .

When discussing the time integration using the learned algorithmic function $\psi(y_0, t_0, \xi)$ later in Section 2.2.4, we will consider how to exploit the above properties to simplify the computations.

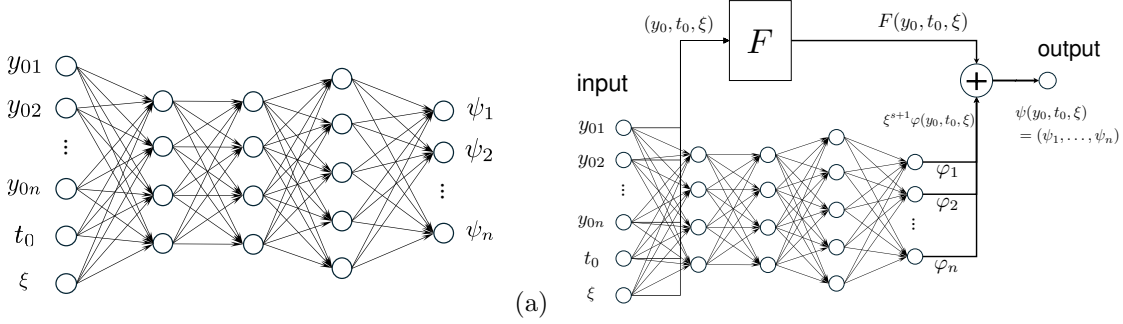


Figure 1: Non-autonomous system: (a) base NN architecture; (b) NN structure adopted in this paper. $F(y_0, t_0, \xi)$ is an approximation of $\psi(y_0, t_0, \xi)$ of s -th order. Three hidden layers are shown as an example.

2.2.2 Representation of Algorithmic Function $\psi(y_0, t_0, \xi)$ by Randomized NNs

We will learn $\psi(y_0, t_0, \xi)$ by solving the system (7) using ELM, for (y_0, t_0, ξ) over some prescribed domain $\Omega \times [T_0, T_f] \times [0, h_{\max}]$, with a physics informed approach. For this purpose, we represent $\psi(y_0, t_0, \xi)$ by an ELM-type randomized feed-forward NN; see Figure 1 for the NN architecture for representing $\psi(y_0, t_0, \xi)$. Figure 1(a) illustrates the base ELM architecture. Let $(L + 1)$ denote the total number of layers in the network, with $L \geq 2$ being an integer. We refer to the vector

$$\mathbf{m} = [m_0, m_1, \dots, m_L] \quad (11)$$

as the architectural vector for this NN, where m_i ($0 \leq i \leq L$) are positive integers corresponding to the number of nodes in layer i . Layer zero is the input layer, representing the input variables (y_0, t_0, ξ) , with $m_0 = n + 2$. Layer L is the output layer, representing the function $\psi(y_0, t_0, \xi)$, with $m_L = n$. The layers in between are the hidden layers. From layer to layer the network logic represents an affine transform, followed by a function composition with an activation function $\sigma : \mathbb{R} \rightarrow \mathbb{R}$ [35]. The coefficients involved in the affine transforms (weights, biases) of different layers are collectively referred to as the network parameters, which may be adjustable (i.e. trainable) or fixed (non-trainable).

ELM distinguishes itself from conventional feed-forward neural networks by the following additional requirements [19, 41]:

- The network parameters in all the hidden layers are pre-assigned to random values and fixed (non-trainable). Specifically, we set the hidden-layer parameters to uniform random values generated on the interval $[-R_m, R_m]$, where R_m is a prescribed constant. Once assigned, these network parameters are fixed throughout the computation.
- The network parameters in the output layer are trainable. They are the ELM training parameters.
- The output layer should contain no activation (i.e. $\sigma(x) = x$), with zero bias.

These ELM requirements are imposed on the NNs when representing $\psi(y_0, t_0, \xi)$ in this paper.

In practice we find it beneficial to incorporate an approximation of ψ explicitly into the NN structure when representing $\psi(y_0, t_0, \xi)$. This is illustrated in Figure 1(b) and is adopted in the current work. The network structure in Figure 1(b) implements the following representation for $\psi(y_0, t_0, \xi)$,

$$\psi(y_0, t_0, \xi) = F(y_0, t_0, \xi) + \xi^{s+1} \varphi(y_0, t_0, \xi), \quad (12)$$

where $F(y_0, t_0, \xi)$ is a prescribed function, s is a prescribed constant, and $\varphi(y_0, t_0, \xi) = (\varphi_1, \dots, \varphi_n) \in \mathbb{R}^n$ denotes a function to be determined and is represented by an ELM-type randomized NN with its architectural vector given by (11).

In this paper we choose $F(y_0, t_0, \xi)$ to be an s -th order approximation of $\psi(y_0, t_0, \xi)$ for some integer s . With this choice the second term in (12), $\xi^{s+1} \varphi$, effectively represents the error of $F(y_0, t_0, \xi)$ in approximating $\psi(y_0, t_0, \xi)$. Therefore, with the NN structure in Figure 1(b), we are effectively learning the error function $\varphi(y_0, t_0, \xi)$, and in turn the function $\psi(y_0, t_0, \xi)$, with ELM. It is noted that by setting $F(y_0, t_0, \xi) = 0$ and $s = -1$ the network in Figure 1(b) reduces to the base NN structure of Figure 1(a).

We consider the following representations of $\psi(y_0, t_0, \xi)$ in this work:

$$s = 0 : F(y_0, t_0, \xi) = y_0, \quad \psi(y_0, t_0, \xi) = y_0 + \xi\varphi(y_0, t_0, \xi); \quad (13a)$$

$$s = 1 : F(y_0, t_0, \xi) = y_0 + \xi f(y_0, t_0), \quad \psi(y_0, t_0, \xi) = y_0 + \xi f(y_0, t_0) + \xi^2\varphi(y_0, t_0, \xi). \quad (13b)$$

For some problems we also consider the following representation,

$$s = 2 : F_1(y_0, t_0, \xi) = f(y_0, t_0), \quad F_2(y_0, t_0, \xi) = f(y_0 + \frac{\xi}{2}F_1, t_0 + \frac{\xi}{2}), \\ F(y_0, t_0, \xi) = y_0 + \xi F_2(y_0, t_0, \xi), \quad \psi(y_0, t_0, \xi) = y_0 + \xi F_2(y_0, t_0, \xi) + \xi^3\varphi(y_0, t_0, \xi). \quad (14)$$

Notice that these representations automatically satisfy the condition in (7b). The $F(y_0, t_0, \xi)$ in (13b) corresponds to a forward Euler approximation of (7a), and that in (14) a mid-point approximation of (7a). In these forms, $\varphi(y_0, t_0, \xi)$ corresponds to the error function of $F(y_0, t_0, \xi)$ and is to be learned by ELM.

Remark 2.1. *In our implementation, the forms of $F(y_0, t_0, \xi)$ and $\psi(y_0, t_0, \xi)$ in (13)-(14) are realized using a lambda layer from the Keras library, in which $\varphi(y_0, t_0, \xi)$ is implemented by a feedforward NN with randomly-assigned and fixed (non-trainable) hidden-layer coefficients. We would like to comment that other representations of $\psi(y_0, t_0, \xi)$ can be formulated, e.g. by choosing $F(y_0, t_0, \xi)$ to be explicit Runge-Kutta approximations of (7a) of higher orders.*

2.2.3 Neural Network Training to Learn Algorithmic Function $\psi(y_0, t_0, \xi)$

We next consider how to train the neural network to learn $\psi(y_0, t_0, \xi)$. Our training is based on a physics-informed approach, employing the nonlinear least squares method [2].

We employ the NN structure from Figure 1(b), corresponding to the representations given in (13)-(14) for $\psi(y_0, t_0, \xi)$. We will refer to the randomized feedforward NN in the lower portion of Figure 1(b), which represents $\varphi(y_0, t_0, \xi)$, as the φ -subnet. The φ -subnet has an architecture characterized by the vector (11).

Let $\phi(y_0, t_0, \xi) = (\phi_1(y_0, t_0, \xi), \phi_2(y_0, t_0, \xi), \dots, \phi_M(y_0, t_0, \xi)) \in \mathbb{R}^M$, where $M = m_{L-1}$, denote the output fields of the last hidden layer of the φ -subnet. Then the network logic of the output layer of the φ -subnet leads to the following relation,

$$\varphi_i(y_0, t_0, \xi) = \sum_{j=1}^M \beta_{ij} \phi_j(y_0, t_0, \xi) = \beta_i \cdot \phi(y_0, t_0, \xi), \quad 1 \leq i \leq n, \quad (15)$$

where $\varphi = (\varphi_1, \varphi_2, \dots, \varphi_n)$, β_{ij} ($1 \leq i \leq n$, $1 \leq j \leq M$) are the weights in the φ -subnet's output layer, and $\beta_i = (\beta_{i1}, \dots, \beta_{iM}) \in \mathbb{R}^M$. Note that β_{ij} are the training parameters of the φ -subnet, and of the overall network for ψ .

The objective here is to train the parameters β_{ij} so that $\psi(y_0, t_0, \xi)$ satisfies (7a) on $y_0 \in \Omega \subset \mathbb{R}^n$, $t_0 \in [T_0, T_f] \subset \mathbb{R}$, and $\xi \in [0, h_{\max}] \subset \mathbb{R}$, for prescribed Ω , T_0 , T_f and h_{\max} . Note that (7b) is automatically satisfied by the NN formulation for $\psi(y_0, t_0, \xi)$.

Define the residual function $R = (R_1, \dots, R_n) \in \mathbb{R}^n$ of the problem,

$$R(\beta, y_0, t_0, \xi) = \frac{\partial \psi}{\partial \xi} - f(\psi, t_0 + \xi), \quad (16)$$

where ψ is given by (12) and (13)-(14), $\beta = (\beta_1, \beta_2, \dots, \beta_n) = (\beta_{11}, \dots, \beta_{1M}, \beta_{21}, \dots, \beta_{nM}) \in \mathbb{R}^{nM}$, and the dependence of R on β has been made explicit. We choose a set of Q points, $(y_0^{(i)}, t_0^{(i)}, \xi^{(i)}) \in \Omega \times [T_0, T_f] \times [0, h_{\max}]$ ($1 \leq i \leq Q$), from a uniform random distribution and refer to them as the collocation points hereafter.

Enforcing $R(\beta, y_0, t_0, \xi)$ to be zero on these collocation points gives rise to the following system,

$$r^{(i)}(\beta) = R(\beta, y_0^{(i)}, t_0^{(i)}, \xi^{(i)}) = \frac{\partial \psi}{\partial \xi} \Big|_{(y_0^{(i)}, t_0^{(i)}, \xi^{(i)})} - f(\psi(y_0^{(i)}, t_0^{(i)}, \xi^{(i)}), t_0^{(i)} + \xi^{(i)}) = 0, \quad 1 \leq i \leq Q, \quad (17)$$

where $r^{(i)} \in \mathbb{R}^n$. This is a system of nonlinear algebraic equations about β , consisting of nQ equations with nM unknowns. Note that, for any given β , the term $\psi(y_0^{(i)}, t_0^{(i)}, \xi^{(i)})$ can be computed by an evaluation of the neural network, and the term $\frac{\partial \psi}{\partial \xi} \Big|_{(y_0^{(i)}, t_0^{(i)}, \xi^{(i)})}$ can be computed by a forward-mode automatic differentiation.

We seek a least squares solution to the algebraic system (17), and determine β by the nonlinear least squares method (i.e. Gauss-Newton method) [2, 3]. Specifically, we compute β using the NLLSQ-perturb (nonlinear least squares with perturbations) algorithm developed in [19]; see also the Appendix A of [22] for a more detailed exposition of NLLSQ-perturb. NLLSQ-perturb employs the scipy implementation of the Gauss-Newton method plus a trust-region strategy (scipy.optimize.least_squares routine) and additionally incorporates a perturbation scheme to keep the method from being trapped to the worst local minima. Upon attaining the least squares solution β by NLLSQ-perturb, we set the output-layer parameters of the φ -subnet by this solution to conclude the NN training. For the NN training, the input data to the network consists of the set of collocation points $(y_0^{(i)}, t_0^{(i)}, \xi^{(i)}) \in \Omega \times [T_0, T_f] \times [0, h_{\max}]$ ($1 \leq i \leq Q$).

To elaborate on the training procedure, the NLLSQ-perturb algorithm [19, 22] requires two routines for its input, one for computing the residual vector $r(\beta) = (\dots, r^{(i)}(\beta), \dots) \in \mathbb{R}^{nQ}$ and the other for computing the Jacobian matrix $\frac{\partial r}{\partial \beta} \in \mathbb{R}^{nQ \times nM}$, for an arbitrary given β . Computing the residual $r^{(i)}(\beta)$ by (17) is straightforward, noting that the terms $\psi(y_0^{(i)}, t_0^{(i)}, \xi^{(i)})$ and $\frac{\partial \psi}{\partial \xi} \Big|_{(y_0^{(i)}, t_0^{(i)}, \xi^{(i)})}$ therein can be attained by forward evaluations of the NN or by automatic differentiations, as discussed above. Computing the Jacobian matrix is more involved. We next discuss its computation and related implementation issues.

To facilitate computation of the Jacobian matrix, we note from (15) and (12) that,

$$\frac{\partial \varphi_i}{\partial \beta_j} = \delta_{ij} \phi(y_0, t_0, \xi) \in \mathbb{R}^{1 \times M}, \quad \frac{\partial \psi_i}{\partial \beta_j} = \xi^{s+1} \frac{\partial \varphi_i}{\partial \beta_j} = \delta_{ij} \xi^{s+1} \phi(y_0, t_0, \xi) \in \mathbb{R}^{1 \times M}, \quad 1 \leq i, j \leq n, \quad (18)$$

where $\psi = (\psi_1, \dots, \psi_n)$ and δ_{ij} denotes the Kronecker delta. In light of (16), for $1 \leq i, j \leq n$,

$$\frac{\partial R_i}{\partial \beta_j} = \frac{\partial}{\partial \xi} \left(\frac{\partial \psi_i}{\partial \beta_j} \right) - \sum_{k=1}^n \frac{\partial f_i}{\partial \psi_k} \frac{\partial \psi_k}{\partial \beta_j} = (s+1) \xi^s \phi \delta_{ij} + \xi^{s+1} \frac{\partial \phi}{\partial \xi} \delta_{ij} - \xi^{s+1} \frac{\partial f_i}{\partial \psi_j} \phi \in \mathbb{R}^{1 \times M}, \quad (19)$$

where $f(\psi, t_0 + \xi) = (f_1, \dots, f_n)$ and we have used (18). So the Jacobian matrix is given by

$$\frac{\partial r}{\partial \beta} = \begin{bmatrix} \frac{\partial r^{(1)}}{\partial \beta_1} & \dots & \frac{\partial r^{(1)}}{\partial \beta_n} \\ \vdots & \ddots & \vdots \\ \frac{\partial r^{(Q)}}{\partial \beta_1} & \dots & \frac{\partial r^{(Q)}}{\partial \beta_n} \end{bmatrix} \in \mathbb{R}^{nQ \times nM}, \quad \frac{\partial r^{(i)}}{\partial \beta_j} = \frac{\partial R}{\partial \beta_j} \Big|_{(y_0^{(i)}, t_0^{(i)}, \xi^{(i)})} = \begin{bmatrix} \frac{\partial R_1}{\partial \beta_j} \Big|_{(y_0^{(i)}, t_0^{(i)}, \xi^{(i)})} \\ \vdots \\ \frac{\partial R_n}{\partial \beta_j} \Big|_{(y_0^{(i)}, t_0^{(i)}, \xi^{(i)})} \end{bmatrix} \in \mathbb{R}^{n \times M}, \quad (20)$$

where $\frac{\partial R_i}{\partial \beta_j}$ is given in (19).

Remark 2.2. *The Jacobian matrix involves the terms like $\phi(y_0^{(i)}, t_0^{(i)}, \xi^{(i)})$ and $\frac{\partial \phi}{\partial \xi} \Big|_{(y_0^{(i)}, t_0^{(i)}, \xi^{(i)})}$, which represent the output fields of the last hidden layer of the φ -subnet and their derivatives. To compute these terms, in our implementation we have created a Keras sub-model of the φ -subnet, which takes (y_0, t_0, ξ) as its input and $\phi(y_0, t_0, \xi)$ (last hidden layer of the φ -subnet) as its output. The terms $\phi(y_0^{(i)}, t_0^{(i)}, \xi^{(i)})$ are then computed by a forward evaluation of this Keras sub-model, and the terms $\frac{\partial \phi}{\partial \xi} \Big|_{(y_0^{(i)}, t_0^{(i)}, \xi^{(i)})}$ are computed by a forward-mode automatic differentiation with this sub-model.*

Remark 2.3. *When the problem (1) becomes more complicated (e.g. being stiff), we find it necessary to incorporate a domain decomposition into the above algorithm for learning $\psi(y_0, t_0, \xi)$. The discussion below pertains to the use of domain decomposition in algorithm learning. Suppose the domain $\Omega \times [T_0, T_f] \subset \mathbb{R}^{n+1}$ is partitioned into N_e ($N_e \geq 1$) non-overlapping sub-domains, $\Omega \times [T_0, T_f] = \mathcal{D}_1 \cup \mathcal{D}_2 \cup \dots \cup \mathcal{D}_{N_e}$. On sub-domain \mathcal{D}_i ($1 \leq i \leq N_e$) we seek a function $\psi_i : \mathcal{D}_i \times [0, h_{\max}] \rightarrow \mathbb{R}^n$ such that*

$$\frac{\partial \psi_i}{\partial \xi} = f(\psi_i(y_0, t_0, \xi), t_0 + \xi), \quad ((y_0, t_0), \xi) \in \mathcal{D}_i \times [0, h_{\max}]; \quad (21a)$$

$$\psi_i(y_0, t_0, 0) = y_0, \quad (y_0, t_0) \in \mathcal{D}_i. \quad (21b)$$

The algorithmic function $\psi(y_0, t_0, \xi)$ for $(y_0, t_0, \xi) \in \Omega \times [T_0, T_f] \times [0, h_{\max}]$ is then given by

$$\psi(y_0, t_0, \xi) = \begin{cases} \psi_1(y_0, \xi), & (y_0, t_0) \in \mathcal{D}_1; \\ \psi_2(y_0, t_0, \xi), & (y_0, t_0) \in \mathcal{D}_2; \\ \dots & \\ \psi_{N_e}(y_0, t_0, \xi), & (y_0, t_0) \in \mathcal{D}_{N_e}. \end{cases} \quad (22)$$

We use a local NN with an architecture given by Figure 1(b) to learn each $\psi_i(y_0, t_0, \xi)$, by solving the system (21) on $\mathcal{D}_i \times [0, h_{\max}]$, for $1 \leq i \leq N_e$. This local learning problem on $\mathcal{D}_i \times [0, h_{\max}]$ is essentially the same as (7). Hence the same algorithm as presented above can be used to learn ψ_i ($1 \leq i \leq N_e$), noting that here the random collocation points shall be taken from $\mathcal{D}_i \times [0, h_{\max}]$. We would like to emphasize that the learning problems on different sub-domains are not coupled, and they can be computed individually or in parallel. In our implementation we have created N_e local ELM-type randomized NNs, implemented as Keras sub-models, with each for one sub-domain. The local NNs each assumes a structure as given by Figure 1(b). They are trained individually in an un-coupled fashion, using the procedure discussed in this section. The learned time-marching algorithm is represented by the collection of these local NNs.

Remark 2.4. The expressions (12) and (13)-(14) are explicit representations of $\psi(y_0, t_0, \xi)$. Given (y_0, t_0, ξ) , $\psi(y_0, t_0, \xi)$ can be explicitly computed by a forward NN evaluation. It is also possible to learn $\psi(y_0, t_0, \xi)$ by adopting an implicit representation, which would entail solving algebraic systems during training and also during time marching, in addition to forward NN evaluations. Therefore, implicit representations of $\psi(y_0, t_0, \xi)$ lead to implicit time integration algorithms. There are several ways to represent $\psi(y_0, t_0, \xi)$ implicitly. One simple idea is to again adopt the representation (12) and (13)-(14) with the same NN as in Figure 1(b), but restrict ξ to the domain $\xi \in [-h_{\max}, 0]$ during NN training. This amounts to an algorithm that marches backward in time, giving rise to an implicit time integration scheme. The procedure discussed in this section, with $\xi \in [-h_{\max}, 0]$, can train the NN for learning this implicit scheme.

We next discuss another implicit representation of $\psi(y_0, t_0, \xi)$, by leveraging implicit Runge-Kutta type approximations. Let us consider

$$\psi(y_0, t_0, \xi) = G(y_0, t_0, \xi) + \xi^{s+1} \varphi(y_0, t_0, \xi), \quad (23)$$

where $G(y_0, t_0, \xi)$ is an s -th order implicit approximation of $\psi(y_0, t_0, \xi)$ in equation (7a). We consider the following specific forms,

$$s = 1: \quad \begin{aligned} K(y_0, t_0, \xi) &= f(y_0 + \xi K(y_0, t_0, \xi), t_0 + \xi), \\ G(y_0, t_0, \xi) &= y_0 + \xi K(y_0, t_0, \xi), \quad \psi(y_0, t_0, \xi) = y_0 + \xi K(y_0, t_0, \xi) + \xi^2 \varphi(y_0, t_0, \xi); \end{aligned} \quad (24a)$$

$$s = 2: \quad \begin{aligned} K_1(y_0, t_0, \xi) &= f(y_0 + \gamma \xi K_1(y_0, t_0, \xi), t_0 + \gamma \xi), \\ K_2(y_0, t_0, \xi) &= f(y_0 + (1 - \gamma) \xi K_1(y_0, t_0, \xi) + \gamma \xi K_2(y_0, t_0, \xi), t_0 + \xi), \\ G(y_0, t_0, \xi) &= y_0 + (1 - \gamma) \xi K_1(y_0, t_0, \xi) + \gamma \xi K_2(y_0, t_0, \xi), \\ \psi(y_0, t_0, \xi) &= y_0 + (1 - \gamma) \xi K_1(y_0, t_0, \xi) + \gamma \xi K_2(y_0, t_0, \xi) + \xi^3 \varphi(y_0, t_0, \xi); \end{aligned} \quad (24b)$$

where $\gamma = 1 - \frac{\sqrt{2}}{2}$. The form (24a) utilizes the first-order backward Euler approximation in the implicit Runge-Kutta form, and (24b) uses the 2nd-order diagonally implicit Runge-Kutta (DIRK) approximation [38, 46]. These representations automatically satisfy (7b). In (23), $\varphi(y_0, t_0, \xi)$ is to be determined, and is represented by an ELM-type randomized NN. This leads to the relation (15), in which β_{ij} are the trainable parameters and $\phi(y_0, t_0, \xi) \in \mathbb{R}^M$ are the output fields of the last hidden layer of the NN. To train this NN, we seek β_{ij} such that the expression (23) for $\psi(y_0, t_0, \xi)$ satisfies (7a), in the least squares sense, on Q random collocation points $(y_0^{(i)}, t_0^{(i)}, \xi^{(i)}) \in \Omega \times [T_0, T_f] \times [0, h_{\max}]$ ($1 \leq i \leq Q$). We can similarly compute β_{ij} by the NLLSQ-perturb algorithm. In this case the residual function is defined by (16) and the residuals on the collocation points are given by (17), where $\psi(y_0, t_0, \xi)$ is given by (23).

Let us use the form (24a) to illustrate how to compute the residual vector $r(\beta) \in \mathbb{R}^{nQ}$ and the Jacobian matrix $\frac{\partial r}{\partial \beta} \in \mathbb{R}^{nQ \times nM}$ for use by NLLSQ-perturb during training. The representation (24b) requires a procedure similar to what follows. With (24a) the residual (17) is reduced to

$$r^{(i)}(\beta) = K(y_0^{(i)}, t_0^{(i)}, \xi^{(i)}) + \xi^{(i)} \frac{\partial K}{\partial \xi} \Big|_{(y_0^{(i)}, t_0^{(i)}, \xi^{(i)})} + 2\xi^{(i)} \varphi(y_0^{(i)}, t_0^{(i)}, \xi^{(i)}) + (\xi^{(i)})^2 \frac{\partial \varphi}{\partial \xi} \Big|_{(y_0^{(i)}, t_0^{(i)}, \xi^{(i)})} - f(\psi(y_0^{(i)}, t_0^{(i)}, \xi^{(i)}), t_0^{(i)} + \xi^{(i)}), \quad 1 \leq i \leq Q. \quad (25)$$

Here $K(y_0^{(i)}, t_0^{(i)}, \xi^{(i)}) \in \mathbb{R}^n$ is computed by solving the nonlinear equation (see the first equation of (24a))

$$K(y_0^{(i)}, t_0^{(i)}, \xi^{(i)}) = f(y_0^{(i)} + \xi^{(i)} K, t_0^{(i)} + \xi^{(i)}). \quad (26)$$

In our implementation we solve this equation using the routine “root” in the scipy library (`scipy.optimize.root`).

$\frac{\partial K}{\partial \xi} \Big|_{(y_0^{(i)}, t_0^{(i)}, \xi^{(i)})} \in \mathbb{R}^n$ in (25) is computed by solving the linear algebraic system

$$\left(\mathbf{I} - \xi^{(i)} \frac{\partial f}{\partial G} \Big|_{(y_0^{(i)}, t_0^{(i)}, \xi^{(i)})} \right) \frac{\partial K}{\partial \xi} \Big|_{(y_0^{(i)}, t_0^{(i)}, \xi^{(i)})} = \frac{\partial f}{\partial G} \Big|_{(y_0^{(i)}, t_0^{(i)}, \xi^{(i)})} K(y_0^{(i)}, t_0^{(i)}, \xi^{(i)}) + \frac{\partial f}{\partial t} \Big|_{(y_0^{(i)}, t_0^{(i)}, \xi^{(i)})}, \quad (27)$$

where $\mathbf{I} \in \mathbb{R}^{n \times n}$ is the identity matrix, $G = y_0 + \xi K(y_0, t_0, \xi)$, $t = t_0 + \xi$, and $f = f(G, t) = f(y_0 + \xi K, t_0 + \xi)$. This linear system results from the differentiation of the first equation in (24a) with respect to ξ . We solve this system using the routine “solve” from the scipy library (`scipy.linalg.solve`). The terms $\varphi(y_0^{(i)}, t_0^{(i)}, \xi^{(i)})$ and $\frac{\partial \varphi}{\partial \xi} \Big|_{(y_0^{(i)}, t_0^{(i)}, \xi^{(i)})}$ in (25) are computed by a forward evaluation of the NN and by a forward-mode automatic differentiation. The Jacobian matrix $\frac{\partial r}{\partial \beta}$ is given by (20), in which

$$\frac{\partial R_i}{\partial \beta_j} = 2\xi \phi(y_0, t_0, \xi) \delta_{ij} + \xi^2 \frac{\partial \phi}{\partial \xi} \delta_{ij} - \xi^2 \frac{\partial f_i}{\partial \psi_j} \phi(y_0, t_0, \xi), \quad (28)$$

to be evaluated on the collocation points. In summary, given $(y_0^{(i)}, t_0^{(i)}, \xi^{(i)})$ ($1 \leq i \leq Q$) and an arbitrary β , we take the following steps to compute $r(\beta)$ and $\frac{\partial r}{\partial \beta}$:

- (i) Compute $\varphi(y_0^{(i)}, t_0^{(i)}, \xi^{(i)})$, $\frac{\partial \varphi}{\partial \xi} \Big|_{(y_0^{(i)}, t_0^{(i)}, \xi^{(i)})}$, $\phi(y_0^{(i)}, t_0^{(i)}, \xi^{(i)})$ and $\frac{\partial \phi}{\partial \xi} \Big|_{(y_0^{(i)}, t_0^{(i)}, \xi^{(i)})}$ by forward valuations of the neural network and by automatic differentiations;
- (ii) Solve equation (26) for $K(y_0^{(i)}, t_0^{(i)}, \xi^{(i)})$;
- (iii) Solve the linear system (27) for $\frac{\partial K}{\partial \xi} \Big|_{(y_0^{(i)}, t_0^{(i)}, \xi^{(i)})}$;
- (iv) Compute $\psi(y_0^{(i)}, t_0^{(i)}, \xi^{(i)})$ by the second equation in (24a);
- (v) Compute $r(\beta)$ by (25);
- (vi) Compute $\frac{\partial r}{\partial \beta}$ by (20) and (28).

Remark 2.5. Hereafter, we refer to the learned NN algorithms employing the explicit formulations (13a), (13b), and (14) as “NN-Exp-S0”, “NN-Exp-S1”, and “NN-Exp-S2”, respectively. We refer to those based on the implicit formulations (24a) and (24b) as “NN-Imp-S1” and “NN-Imp-S2”, respectively.

2.2.4 Time Marching Based on Learned Algorithmic Function $\psi(y_0, t_0, \xi)$

With appropriately chosen domain $\Omega \times [T_0, T_f] \times [0, h_{\max}]$ for network training, the trained ELM network can be used as a time marching algorithm for solving problem (1), with arbitrary initial data $(y_0, t_0) \in \Omega \times [T_0, T_f]$ and step size $h \in (0, h_{\max})$.

Let $\psi_\beta(y_0, t_0, \xi)$ denote the learned algorithmic function represented by the trained neural network. Suppose the initial time and data are (t_0, y_0) , h is the step size, and y_k is the approximation to the solution at $t_k = t_0 + kh$ ($k \geq 0$). Given (y_k, t_k) , we compute the solution at $t_{k+1} = t_k + h$ by

$$y_{k+1} = \psi_\beta(y_k, t_k, h), \quad k \geq 0. \quad (29)$$

It can be noted that only forward NN evaluations are needed for solving IVPs if the learned algorithm is based on an explicit representation of $\psi(y_0, t_0, \xi)$. On the other hand, if the algorithm is based on an implicit representation (see Remark 2.4), solving an algebraic system is required during time marching, apart from the forward NN evaluations. We will elaborate on the implicit case in a remark (Remark 2.11) below.

Since one is not able to learn the algorithmic function $\psi(y_0, t_0, \xi)$ perfectly, due to practical constraints (such as space, time, and computational resource), it should be emphasized that the learned algorithm $\psi_\beta(y_0, t_0, \xi)$ is but an approximation of the exact time integration algorithm $\psi(y_0, t_0, \xi)$. Nonetheless, we observe that the learned algorithms are highly competitive, in terms of their accuracy and time marching cost, compared with the leading traditional time integration algorithms. This point will be demonstrated with numerical experiments in Section 3.

Remark 2.6. Choosing an appropriate domain $\Omega \times [T_0, T_f] \times [0, h_{\max}]$, from which the collocation points are drawn, for training the NN is important to the accuracy of the learned algorithm $\psi_{\beta}(y_0, t_0, \xi)$. In general the domain Ω and $[T_0, T_f]$ should be sufficiently large so that $y_k \in \Omega$ and $t_k \in [T_0, T_f]$ for all $0 \leq k \leq N$ (N denoting the number of time steps one plans to perform), and the parameter h_{\max} should be sufficiently large so that the step size h of interest falls in $(0, h_{\max})$. On the other hand, an overly large Ω , $(T_f - T_0)$, or h_{\max} can increase the difficulty in the network training. In this regard, some knowledge about the system to be simulated can be helpful to the choice of Ω , h_{\max} , and $[T_0, T_f]$. In the absence of any knowledge about the system, preliminary simulations are useful for making a choice about Ω , h_{\max} and $[T_0, T_f]$.

Remark 2.7. Suppose one intends to solve the non-autonomous system (1) for $0 \leq t \leq t_f$, with $t_0 = 0$ in (1b) and t_f being large (long time integration). When training the NN, the domain $[T_0, T_f]$ should in general be chosen to be at least $[0, t_f]$. Since t_f is large, using a single NN to accurately learn $\psi(y_0, t_0, \xi)$ on $(y_0, t_0, \xi) \in \Omega \times [0, t_f] \times [0, h_{\max}]$ can become very challenging. To alleviate this problem, one can incorporate a domain decomposition of $[0, t_f]$ and employ local NNs to learn ψ on the sub-domains (see Remark 2.3). Let us suppose $[0, t_f]$ is partitioned into m ($m \geq 1$) sub-domains with $0 = T_0 < T_1 < \dots < T_m = t_f$. One only needs to train m local NNs, each for a sub-domain $t_0 \in [T_{i-1}, T_i]$ ($1 \leq i \leq m$), individually in an un-coupled fashion. By using a moderate size for the sub-domains, training the local NNs would become significantly easier. By incorporating domain decomposition and local neural networks, one can effectively learn the time marching algorithm for solving non-autonomous systems over long time horizons.

Remark 2.8. In the presence of domain decomposition (see Remark 2.3), the algorithm (29) needs to be modified accordingly for time integration. Let $\psi_{\beta_i}(y_0, t_0, \xi)$ denote the learned $\psi_i(y_0, t_0, \xi)$ on the sub-domain $\mathcal{D}_i \times [0, h_{\max}]$ for $1 \leq i \leq N_e$. Then given (y_k, t_k) we approximate the solution at $t_{k+1} = t_k + h$ by

$$\begin{aligned} (i) & \text{ determine } s \ (1 \leq s \leq N_e) \text{ such that } (y_k, t_k) \in \mathcal{D}_s; \\ (ii) & \ y_{k+1} = \psi_{\beta_s}(y_k, t_k, h). \end{aligned} \tag{30}$$

In the event (y_k, t_k) falls on the shared boundary of two or more sub-domains, one can choose the ψ_{β} corresponding to any of these sub-domains for time integration. In our implementation, we have used the sub-domain with the lowest ID for time integration. To reduce the influence of different choices of sub-domains in such cases, during NN training it is preferable, after the domain $\Omega \times [T_0, T_f]$ is partitioned into disjoint sub-domains \mathcal{D}_i , to enlarge each sub-domain slightly (e.g. by a few percent) along the directions of domain decomposition. In this way, $\psi_i(y_0, t_0, \xi)$ will be learned/trained on a domain slightly larger than \mathcal{D}_i . To be more specific, suppose the sub-domain \mathcal{D}_i has a dimension $[a, b]$ along a direction with domain decomposition, and let $r \geq 0$ denote the enlargement factor. Then along this direction the enlarged sub-domain for NN training will have a dimension $[a - (b - a)\frac{r}{2}, b + (b - a)\frac{r}{2}]$. Note that the use of enlarged sub-domains is for network training only. During time marching, the algorithm (30) will still choose the algorithmic function based on the disjoint partitions \mathcal{D}_i .

Remark 2.9. If $f(y, t)$ in (1) is periodic in t with the period T , as shown by Theorem 2.3, it would be sufficient to learn $\psi(y_0, t_0, \xi)$ on $(y_0, t_0, \xi) \in \Omega \times [T_0, T_f] \times [0, h_{\max}]$, with $[T_0, T_f]$ covering one period of $f(y, t)$, and the learned algorithm $\psi_{\beta}(y_0, t_0, \xi)$ can be used to solve system (1) for all $t \in \mathbb{R}$ (arbitrarily long time horizons). This property can significantly simplify the algorithm learning and the long-time integration of non-autonomous systems with a periodic RHS. In this case, time integration using the learned algorithm $\psi_{\beta}(y_0, t_0, \xi)$, which is trained on $(y_0, t_0, \xi) \in \Omega \times [0, T] \times [0, h_{\max}]$, takes the following form. Given (y_k, t_k) with $t_k \in \mathbb{R}$, we compute (y_{k+1}, t_{k+1}) by,

$$y_{k+1} = \psi_{\beta}(y_k, t_k^*, h), \quad t_k^* = \text{mod}(t_k, T), \quad t_{k+1} = t_k + h, \tag{31}$$

where mod denotes the modulo operation.

Remark 2.10. If $f(y, t)$ in (1) is periodic with respect to one or more components of $y \in \mathbb{R}^n$, when learning $\psi(y_0, t_0, \xi)$ on $(y_0, t_0, \xi) \in \Omega \times [T_0, T_f] \times [0, h_{\max}]$, it would be sufficient to choose Ω to cover one period of $f(y, t)$ along those directions, as shown by Theorem 2.4. The resultant algorithm can be used to solve the system (1) with those components of $y_0 \in \mathbb{R}^n$ in the periodic directions taking arbitrary values.

Define a constant vector $\mathbf{L} = (L_1, \dots, L_n) \in \mathbb{R}^n$ with $L_i \geq 0$ ($1 \leq i \leq n$) and assume $\mathbf{L} \neq \mathbf{0}$. Suppose

$$f(y + L_i \mathbf{e}_i, t) = f(y, t), \quad \text{for all } (y, t) \in \mathbb{R}^n \times \mathbb{R}, \quad 1 \leq i \leq n. \tag{32}$$

If $L_i > 0$ ($1 \leq i \leq n$), equation (32) indicates that $f(y, t)$ is periodic with respect to y_i with a period L_i . If $L_i = 0$, equation (32) is reduced to an identity and we use this to denote that $f(y, t)$ is not periodic with respect to y_i . We will refer to \mathbf{L} as the periodicity vector of $f(y, t)$ hereafter.

Given the periodicity vector $\mathbf{L} = (L_1, \dots, L_n)$ for $f(y, t)$, we suppose the NN has been trained to learn $\psi(y_0, t_0, \xi)$ on $\Omega \times [T_0, T_f] \times [0, h_{\max}]$, where Ω covers one period of $f(y, t)$ along those periodic directions. Solving system (1) based on the learned algorithm $\psi_{\beta}(y_0, t_0, \xi)$ takes the following form. Given step size h and (y_k, t_k) , where $y_k = (y_{k1}, \dots, y_{kn})$,

(i) for $i = 1, \dots, n$:

$$\text{if } L_i > 0, \text{ then set } y_{ki}^* = \text{mod}(y_{ki}, L_i) \text{ and } q_i = \left\lfloor \frac{y_{ki}}{L_i} \right\rfloor;$$

$$\text{else set } y_{ki}^* = y_{ki} \text{ and } q_i = 0.$$

(ii) $y_{k+1} = \psi_{\beta}(y_k^*, t_k, h) + \text{mult}(q, \mathbf{L})$, where $y_k^* = (y_{k1}^*, \dots, y_{kn}^*)$, $q = (q_1, \dots, q_n) \in \mathbb{Z}^n$, and $\text{mult}(\cdot, \cdot)$ denotes the element-wise multiplication of two vectors and returns the resultant vector.

In the above steps $\lfloor \cdot \rfloor$ denotes the floor function.

Remark 2.11. Implicit representations of $\psi(y_0, t_0, \xi)$ (see Remark 2.4) lead to implicit time integration algorithms for solving (1). For an implicit NN algorithm ψ_{β} trained on $(y_0, t_0, \xi) \in \Omega \times [T_0, T_f] \times [-h_{\max}, 0]$, given (y_k, t_k) and step size $h \in (0, h_{\max})$, the solution y_{k+1} at $t_{k+1} = t_k + h$ is determined by

$$y_k = \psi_{\beta}(y_{k+1}, t_{k+1}, -h). \quad (33)$$

This is a nonlinear system of algebraic equations involving the NN function ψ_{β} , which needs to be solved for y_{k+1} . This system can be solved using the scipy routine “root” (`scipy.optimize.root`) in the implementation, in which the Jacobian matrix can be computed by automatic differentiation. For NN algorithms based on the implicit representations (24a) and (24b), time marching takes the following forms: given (y_k, t_k) and h ,

$$K = f(y_k + hK, t_k + h), \quad y_{k+1} = y_0 + hK + h^2 \varphi_{\beta}(y_k, t_k, h); \quad (34)$$

and

$$K_1 = f(y_k + \gamma h K_1, t_k + \gamma h), \quad K_2 = f(y_k + (1 - \gamma)h K_1 + \gamma h K_2, t_k + h), \quad (35a)$$

$$y_{k+1} = y_k + (1 - \gamma)h K_1 + \gamma h K_2 + h^3 \varphi_{\beta}(y_k, t_k, h). \quad (35b)$$

Here φ_{β} denotes the function $\varphi(y_0, t_0, \xi)$ in (24a) and (24b) learned by the neural network. Nonlinear equations need to be solved for computing K , K_1 , and K_2 during time marching. They can be solved based on the scipy routine “root” in the implementation.

2.3 Learning Exact Time Marching Algorithm for Autonomous Systems

If system (1) is autonomous, the algorithm presented in the previous subsection will be simplified. We briefly discuss this case here. Consider an autonomous system in (1), i.e.

$$\frac{dy}{dt} = f(y), \quad (36)$$

where $f: \mathbb{R}^n \rightarrow \mathbb{R}^n$ is a prescribed function, together with the initial condition (1b).

By again introducing the transformation (4), we re-write the system consisting of (36) and (1b) into

$$\frac{dY}{d\xi} = f(Y), \quad (37a)$$

$$Y(0) = y_0. \quad (37b)$$

The solution to problem (37) depends only on y_0 and ξ , and we re-write it as $Y(\xi) = \psi(y_0, \xi)$ to make the dependence on y_0 and ξ explicit. $\psi(y_0, \xi)$ is the algorithmic function for the system consisting of (36) and (1b). This function is determined by,

$$\frac{\partial \psi}{\partial \xi} = f(\psi(y_0, \xi)), \quad (38a)$$

$$\psi(y_0, 0) = y_0. \quad (38b)$$

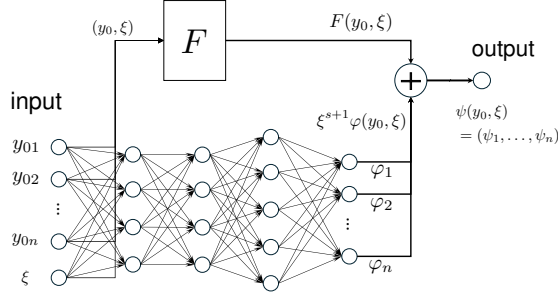


Figure 2: Autonomous system: neural network structure, with three hidden layers shown as an example.

We learn the function $\psi(y_0, \xi)$, for $(y_0, \xi) \in \Omega \times [0, h_{\max}]$, by solving the system (38) with ELM, for prescribed Ω and h_{\max} . The trained NN can be used to solve the problem consisting of (36) and (1b).

Figure 2 illustrates the NN structure employed to learn $\psi(y_0, \xi)$, which implements the following representation,

$$\psi(y_0, \xi) = F(y_0, \xi) + \xi^{s+1} \varphi(y_0, \xi), \quad (39)$$

where $F(y_0, \xi) \in \mathbb{R}^n$ is a prescribed s -th order approximation of $\psi(y_0, \xi)$ (for some integer s), and $\varphi(y_0, \xi) \in \mathbb{R}^n$ is an unknown function represented by the ELM-type randomized NN. The NN input nodes represent $(y_0, \xi) \in \mathbb{R}^n \times \mathbb{R}$, and the output nodes represent $\psi(y_0, \xi) \in \mathbb{R}^n$. We again refer to the portion of the network representing $\varphi(y_0, \xi)$ as the φ -subset. The φ -subset has an architecture characterized by (11), with $m_0 = n + 1$ and $m_L = n$ and its hidden-layer coefficients randomly assigned and fixed.

Analogous to (13) and (14), we consider the following representations for $\psi(y_0, \xi)$:

$$s = 0 : \quad F(y_0, \xi) = y_0, \quad \psi(y_0, \xi) = y_0 + \xi \varphi(y_0, \xi); \quad (40a)$$

$$s = 1 : \quad F(y_0, \xi) = y_0 + \xi f(y_0), \quad \psi(y_0, \xi) = y_0 + \xi f(y_0) + \xi^2 \varphi(y_0, \xi); \quad (40b)$$

and for some problems also

$$s = 2 : \quad F_1(y_0, \xi) = f(y_0), \quad F_2(y_0, \xi) = f(y_0 + \frac{\xi}{2} F_1), \\ F(y_0, \xi) = y_0 + \xi F_2(y_0, \xi), \quad \psi(y_0, \xi) = y_0 + \xi F_2(y_0, \xi) + \xi^3 \varphi(y_0, \xi). \quad (41)$$

These forms automatically satisfy (38b). Therefore, only (38a) needs to be considered for NN training.

We train the NN such that $\psi(y_0, \xi)$ satisfies (38a) for $y_0 \in \Omega$ and $\xi \in [0, h_{\max}]$. The procedure from Section 2.2.3 can be adapted to train the NN here for autonomous systems. The logic of the φ -subset's output layer gives rise to a relation analogous to (15),

$$\varphi_i(y_0, \xi) = \beta_i \cdot \phi(y_0, \xi), \quad 1 \leq i \leq n, \quad (42)$$

where $\varphi(y_0, \xi) = (\varphi_1, \dots, \varphi_n) \in \mathbb{R}^n$, $\phi(y_0, \xi) = (\phi_1, \dots, \phi_M) \in \mathbb{R}^M$, $M = m_{L-1}$ denoting the number of nodes in the last hidden layer of the φ -subset, and $\beta_i = (\beta_{i1}, \dots, \beta_{iM}) \in \mathbb{R}^M$ for $1 \leq i \leq n$. Note that $\varphi(y_0, \xi)$ is the output field of the φ -subset and $\phi(y_0, \xi)$ denotes the output fields of the last hidden layer of the φ -subset. β_{ij} ($1 \leq i \leq n$, $1 \leq j \leq M$) are the training parameters of the network.

We determine the training parameters $\beta = (\beta_1, \dots, \beta_n) = (\beta_{11}, \dots, \beta_{1M}, \beta_{21}, \dots, \beta_{nM}) \in \mathbb{R}^{nM}$ by the nonlinear least squares method. Let $(y_0^{(i)}, \xi^{(i)})$ ($1 \leq i \leq Q$) denote Q random collocation points on $\Omega \times [0, h_{\max}]$ drawn from a uniform distribution. Enforcing (38a) on these collocation points leads to the following nonlinear algebraic system about β ,

$$r^{(i)}(\beta) = \frac{\partial \psi}{\partial \xi} \Big|_{(y_0^{(i)}, \xi^{(i)})} - f(\psi(y_0^{(i)}, \xi^{(i)})) = 0, \quad 1 \leq i \leq Q, \quad (43)$$

in which ψ is given by (40)-(41) and (42) and the dependence of the residual $r^{(i)} \in \mathbb{R}^n$ on β is made explicit. This is a system of nQ nonlinear algebraic equations about nM unknowns. We seek a least squares

solution to this system and compute β by the NLLSQ-perturb algorithm [19, 22]. NLLSQ-perturb requires the computation of the residual vector and the Jacobian matrix for arbitrary given β , as noted previously. Computing the residual vector $r(\beta) = (r^{(1)}, \dots, r^{(Q)}) \in \mathbb{R}^{nQ}$ for NLLSQ-perturb is straightforward in light of (43), noting that $\psi(y_0^{(i)}, \xi^{(i)})$ and $\frac{\partial \psi}{\partial \xi} \Big|_{(y_0^{(i)}, \xi^{(i)})}$ therein can be obtained by forward NN evaluations and by automatic differentiation. The Jacobian matrix is given by

$$\frac{\partial r}{\partial \beta} = \begin{bmatrix} \frac{\partial r^{(1)}}{\partial \beta_1} & \cdots & \frac{\partial r^{(1)}}{\partial \beta_n} \\ \vdots & \ddots & \vdots \\ \frac{\partial r^{(Q)}}{\partial \beta_1} & \cdots & \frac{\partial r^{(Q)}}{\partial \beta_n} \end{bmatrix} \in \mathbb{R}^{nQ \times nM}, \quad \frac{\partial r^{(i)}}{\partial \beta_j} = \begin{bmatrix} \frac{\partial r_1^{(i)}}{\partial \beta_j} \\ \vdots \\ \frac{\partial r_n^{(i)}}{\partial \beta_j} \end{bmatrix} \in \mathbb{R}^{n \times M}, \quad (44)$$

where

$$\begin{aligned} \frac{\partial r_k^{(i)}}{\partial \beta_j} &= (s+1)(\xi^{(i)})^s \phi(y_0^{(i)}, \xi^{(i)}) \delta_{kj} + (\xi^{(i)})^{s+1} \frac{\partial \phi}{\partial \xi} \Big|_{(y_0^{(i)}, \xi^{(i)})} \delta_{kj} \\ &\quad - (\xi^{(i)})^{s+1} \frac{\partial f_k}{\partial \psi_j} \Big|_{(y_0^{(i)}, \xi^{(i)})} \phi(y_0^{(i)}, \xi^{(i)}) \in \mathbb{R}^{1 \times M}, \quad 1 \leq i \leq Q, 1 \leq k, j \leq n. \end{aligned} \quad (45)$$

The terms $\phi(y_0^{(i)}, \xi^{(i)})$ and $\frac{\partial \phi}{\partial \xi} \Big|_{(y_0^{(i)}, \xi^{(i)})}$ involved in the Jacobian matrix can be computed by forward evaluations of a network sub-model and by automatic differentiations (see Remark 2.2).

The trained NN contains the learned algorithm for solving the system consisting of (36) and (1b), with any initial condition $y_0 \in \Omega$, initial time $t_0 \in \mathbb{R}$, and step size $h \in (0, h_{\max})$. Suppose (y_k, t_k) provide the solution and the time at step k ($k \geq 0$), and that $\psi_\beta(y_0, \xi)$ denotes the learned algorithmic function. The solution at the new time step is given by (h denoting the step size),

$$y_{k+1} = \psi_\beta(y_k, h), \quad t_{k+1} = t_k + h, \quad (46)$$

which involves the forward evaluation of the neural network.

Remark 2.12. *The discussion on implicit representations of ψ for non-autonomous systems in Remarks 2.4 and 2.11 can be adapted to autonomous systems for learning and using $\psi(y_0, \xi)$. The equations (23) and (24) and other related expressions need to be modified accordingly to exclude the t_0 effects.*

3 Computational Examples

In this section we evaluate the performance of the learned time integration algorithms from Section 2 by simulating the dynamics of several non-autonomous and autonomous systems. Some of these systems are chaotic, or can become stiff for a range of problem parameters. In particular, we compare the learned NN algorithms with the leading traditional time integration algorithms as implemented in the Scipy library (scipy.integrate.solve_ivp routine, with methods ‘‘DOP853’’, ‘‘RK45’’, ‘‘RK23’’, ‘‘Radau’’ and ‘‘BDF’’) in terms of the solution accuracy and the time marching cost. All the scipy methods are adaptive in the step size and in the integration order, with ‘‘DOP853’’, ‘‘RK45’’, and ‘‘RK23’’ being explicit and ‘‘Radau’’ and ‘‘BDF’’ being implicit schemes. With the learned NN algorithms, we employ a constant time step size for the majority of simulations, and a quasi-adaptive time step for certain stiff cases.

We define the maximum error e_{\max} and the root-mean-squares (rms) error e_{rms} of a solution $y(t) = (y_1(t), y_2(t), \dots, y_n(t)) \in \mathbb{R}^n$ for $t \in [t_0, t_f]$ as follows,

$$e_{\max} = \max\{ \max\{ |y_i^c(t_j) - y_i^{ex}(t_j)| \}_{j=1}^m \}_{i=1}^n, \quad e_{\text{rms}} = \sqrt{\frac{1}{mn} \sum_{i=1}^n \sum_{j=1}^m |y_i^c(t_j) - y_i^{ex}(t_j)|^2}. \quad (47)$$

Here y^c is the numerical solution obtained by the NN algorithms (or the scipy methods), y^{ex} is the exact solution (if available) or a reference solution, and $t_j \in [t_0, t_f]$ ($1 \leq j \leq m$) denotes the time instants resulting

M	current-NN-evaluation (seconds)	keras-NN-evaluation (seconds)
400	0.00138	0.0258
600	0.00148	0.0270
800	0.00155	0.0271

Table 1: Comparison of the time-marching cost (wall time) of NN-Exp-S1 employing (i) the current customized NN evaluation method, and (ii) the Keras built-in NN evaluation method (in graph mode), for the test problem from Section 3.1 ($\lambda = 100$). The tests correspond to those in Figure 5. M is the number of training parameters. The built-in evaluation method calls the Keras model directly with the input data.

from the time marching algorithm corresponding to a constant or a quasi-adaptive time step. When the exact solution is unavailable, the reference solution is computed using the scipy method “DOP853” (for non-stiff problems) or “Radau” (for stiff problems) with absolute tolerance 10^{-16} and relative tolerance 10^{-13} .

For the learned NN algorithms, the time-marching cost lies primarily in the forward evaluation of the trained NN (see (29)) at every time step. Therefore, efficient NN evaluation is critical to the performance of the current NN algorithms. As mentioned before, our implementation is based on the Tensorflow and Keras libraries. We observe that the built-in NN evaluation methods from the Keras library, such as the direct call against a Keras model (or the “predict()” method), even in the graph mode, induces a significant overhead, slowing down the NN time marching.

To reduce the NN evaluation overhead, we have employed a customized evaluation method for the trained NN using routines from the numpy library. Here is the main idea for the customized evaluation. After the neural network is trained, we extract the weight and bias coefficients, as well as the activation functions, for all layers from the trained Keras model. Then we form a routine in which the extracted data are employed to implement the NN logic using plain numpy functions. This routine is used as the customized NN evaluation method for time marching.

We would like to mention another point in our implementation, regarding the computation of $f(y, t)$ for given (y, t) ($y \in \mathbb{R}^n$) in the customized NN evaluation method, which is needed for computing the $F(y_0, t_0, \xi)$ term in (12). We have implemented a routine for computing $f(y, t)$, used specifically for time marching, in which the input data (y, t) is a vector with shape $(n + 1,)$ (in the Python notation). Note that the computation of $f(y, t)$ is also required during NN training, where the input data is a matrix with shape $(N_c, n + 1)$ that represents (y, t) on N_c collocation points. In the version specifically for time marching, the simpler vectorial input data of (y, t) allows more efficient implementation for computing $f(y, t)$.

The learned algorithms employing the above customized NN evaluation method is significantly faster than those based on the built-in evaluation methods from Keras. This point is demonstrated by Table 1, which shows the time-marching time of the NN-Exp-S1 algorithm (see Remark 2.5) for the test problem of Section 3.1 employing the customized NN evaluation method and the Keras built-in method. The algorithm using the customized NN evaluation is faster by more than an order of magnitude.

When implementing the φ -subnet for representing $\varphi(y_0, t_0, \xi)$, we have added a normalization between the input layer (representing (y_0, t_0, ξ)) and the first hidden layer. The normalization implements an affine transform for each component of (y_0, t_0, ξ) , transforming the input (y_0, t_0) data from $[a_1, b_1] \times \dots \times [a_n, b_n] \times [T_1 \times T_2] \subset \mathbb{R}^n \times \mathbb{R}$ to the standard domain $[-1, 1]^n \times [-1, 1]$ and the input ξ data from $[0, h_{\max}]$ to the interval $[0, \frac{1}{\delta_m}]$. Here the prescribed constant $\delta_m > 0$ will be referred to as the ξ -domain map factor, with $\delta_m = 1$ by default. For some stiff problems, we find it more favorable to employ a smaller δ_m with the NN algorithms. These δ_m values will be provided when discussing the specific test problems. The use of δ_m essentially stipulates that the normalization should map the interval $[0, \delta_m h_{\max}]$ to the standard domain $[0, 1]$ for ξ . In the simulations we will employ $\delta_m = 1$, unless otherwise specified. The normalization procedure discussed here is implemented using a “lambda” layer from the Keras library. When domain decomposition is present, the above normalization is implemented for the local NN on each sub-domain. In the simulations we employ no domain decomposition by default, unless otherwise specified.

When the training domain is decomposed along some direction, in Remark 2.8 we have discussed enlarging the sub-domains by a factor r along this direction during network training. In the following numerical tests we employ an enlargement factor $r = 0$ (i.e. no enlargement) by default, unless otherwise specified.

$\lambda = 100$	domain: $(y_0, t_0, \xi) \in [-1.1, 1.1] \times [-0.05, 1.05] \times [0, h_{\max}]$ no domain decomposition r : 0.0 Q : varied Δt : 0.02 (for time marching)	NN: $[3, M, 1]$ (M varied) activation function: Gaussian δ_m : 1 R_m : to be specified time: $t \in [0, 1]$
$\lambda = 10^6$	domain: $(y_0, t_0, \xi) \in [-1.1, 1.1] \times [-0.05, 1.05] \times [0, h_{\max}]$ sub-domains: 2 along t_0 (uniform) r : 0.05 along t_0 Q : 1000 or 900 (random) Δt : 0.02 (for time marching)	NN: $[3, M, 1]$ (M varied) activation function: Gaussian δ_m : 0.02 or 0.01 R_m : to be specified time: $t \in [0, 1]$

Table 2: NN simulation parameters for the linear system (Section 3.1). Values for some parameters are specified in the text.

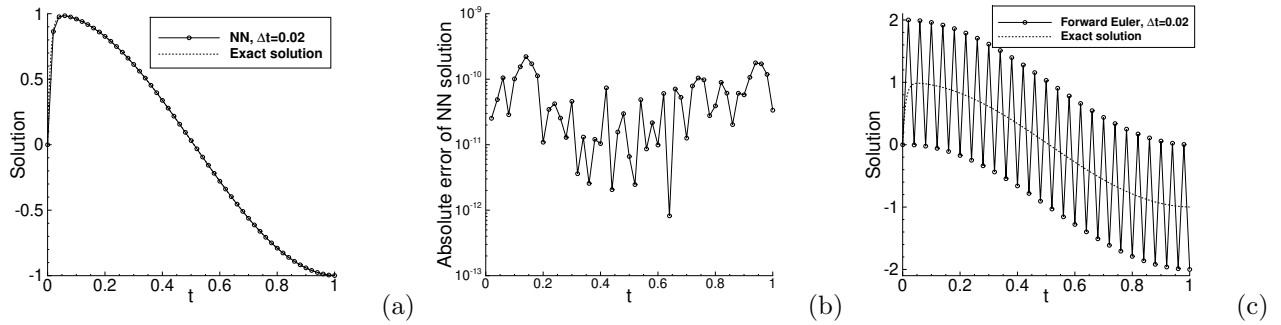


Figure 3: Linear model ($\lambda = 100$): (a) Comparison of $y(t)$ between the NN-Exp-S1 solution and the exact solution. (b) Absolute error history of the NN-Exp-S1 solution. (c) History of $y(t)$ obtained by the forward Euler method (i.e. the $F(y_0, t_0, \xi)$ component in NN-Exp-S1, see (13b)). Training domain: $h_{\max} = 0.03$, NN: $[3, 800, 1]$, $Q = 2500$, and $R_m = 0.5$. See Table 2 for the other parameter values.

3.1 A Linear System: Non-Stiff and Stiff Cases

In this test we consider a linear non-autonomous problem,

$$\frac{dy}{dt} = -\lambda[y - \cos(\pi t)], \quad t \in [0, 1], \quad (48a)$$

$$y(t_0) = y_0, \quad (48b)$$

where $\lambda > 0$ is a constant, $y(t)$ is the unknown to be computed, $t_0 = 0$, and $y_0 = 0$ is the initial condition. This problem becomes very stiff with large λ values. It has the following exact solution,

$$y(t) = \left[y_0 - \frac{\lambda^2}{\lambda^2 + \pi^2} \cos(\pi t_0) - \frac{\lambda\pi}{\lambda^2 + \pi^2} \sin(\pi t_0) \right] e^{-\lambda(t-t_0)} + \frac{\lambda^2}{\lambda^2 + \pi^2} \cos(\pi t) + \frac{\lambda\pi}{\lambda^2 + \pi^2} \sin(\pi t). \quad (49)$$

We use an ELM network with architecture $[3, M, 1]$ and the Gaussian activation function $\sigma(x) = e^{-x^2}$ for the φ -subset to learn the algorithmic function $\psi(y_0, t_0, \xi)$, where M is varied. The hidden-layer coefficients of the φ -subnet are assigned to random values generated on the interval $[-R_m, R_m]$ drawn from a uniform distribution, where the constant R_m is specified below. The NN is trained on a domain $(y_0, t_0, \xi) \in [-1.1, 1.1] \times [-0.05, 1.05] \times [0, h_{\max}]$, where h_{\max} is specified below. We employ Q random collocation points, where Q is varied, uniformly drawn from the domain to train the NN as discussed in Section 2. We employ the trained NN to solve the problem (48) for $t \in [0, 1]$, using a step size $\Delta t = 0.02$ and the initial condition $(y_0, t_0) = (0, 0)$. The maximum and rms errors (e_{\max} , e_{rms}) of the numerical solution against the exact solution (49) are then computed and the time marching cost (wall time) of the NN algorithms is recorded for analysis. Table 2 summarizes the simulation parameters related to the NN algorithms. The same parameters will appear in the subsequent test problems.

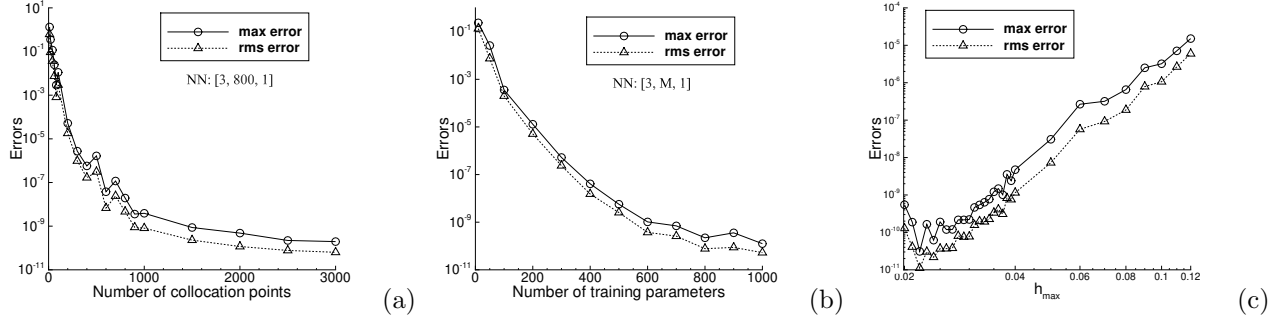


Figure 4: Linear model ($\lambda = 100$): Time marching errors (e_{\max} , e_{rms}) versus (a) the number of training collocation points (Q), (b) the number of training parameters (M) in NN, and (c) the domain size h_{\max} along ξ , obtained with the NN-Exp-S1 algorithm. $h_{\max} = 0.03$ in (a,b) and is varied in (c); $M = 800$ in (a,c) and is varied in (b); $Q = 2500$ in (b,c) and is varied in (a); $R_m = 0.5$; Other simulation parameters are given in Table 2.

We first consider a non-stiff case, with $\lambda = 100$ in (48), and illustrate the characteristics of the learned NN algorithms. Figures 3(a,b) provide an overview of the NN solution, comparing the solution histories from the NN-Exp-S1 algorithm (see Remark 2.5) and the exact solution (49) and showing the absolute-error history of NN-Exp-S1. The parameter values for NN-Exp-S1 are listed in the figure caption or in Table 2. The NN solution is highly accurate, with a maximum error on the order of 10^{-10} over $t \in [0, 1]$. Notice that the NN-Exp-S1 algorithm consists of two components (see (13b)), $F(y_0, t_0, \xi)$ and $\varphi(y_0, t_0, \xi)$, with the former being the forward Euler formula and the latter a neural network correction. We find that the $\varphi(y_0, t_0, \xi)$ component is critical to the NN-Exp-S1 accuracy. Without this component, the solution becomes very poor. Figure 3(c) shows the history of $y(t)$ obtained by the forward Euler method ($\Delta t = 0.02$), i.e. the $F(y_0, t_0, \xi)$ component solely. The numerical solution is highly oscillatory, with no accuracy at all.

Figure 4 illustrates the effects of several simulation parameters on the attained NN algorithm. It shows the maximum and rms time-marching errors of NN-Exp-S1 as a function of the number of collocation points (Q), the number of training parameters (M), and the domain size h_{\max} along ξ , used for training the algorithm. The errors are obtained on the points corresponding to a time step $\Delta t = 0.02$ for $t \in [0, 1]$. The parameter values are specified in the figure caption or Table 2. Each plot represents a group of tests, in which one parameter is varied while the other parameters are fixed when training the NN-Exp-S1 network, and the trained algorithm is employed in time marching to obtain the errors. For example, in Figure 4(a) the number of training collocation points Q is varied systematically when training NN-Exp-S1, while the other parameters are fixed. We observe that the NN errors decrease nearly exponentially with increasing number of collocation points (Q) or training parameters (M). Using a smaller domain along ξ (i.e. smaller h_{\max}) generally leads to improved accuracy in the attained NN algorithm. Numerical experiments suggest that the accuracy of the NN algorithm seems to be determined at the time of training. Once the network is trained, the accuracy of the resultant NN algorithm will be fixed. Varying the step size $\Delta t \in [0, h_{\max}]$ in time marching using the trained NN algorithm appears to have little influence on the time-marching error. This characteristic is somewhat different from traditional numerical algorithms, whose accuracy generally improves with decreasing time step size.

A comparison of the accuracy and the time-marching cost (wall time) of different NN algorithms with explicit (see (13)-(14)) and implicit (see (24)) formulations is provided in Figure 5. These plots show the maximum and rms errors and the time-marching time as a function of the number of training parameters (M) in the NN obtained by NN-Exp-S0, NN-Exp-S1, NN-Exp-S2, NN-Imp-S1, and NN-Imp-S2 (see Remark 2.5). The simulation parameters for this group of tests are specified in the figure caption or in Table 2. Among the explicit NN algorithms, NN-Exp-S2 tends to be more accurate than NN-Exp-S1, which in turn is generally more accurate than NN-Exp-S0. In terms of time-marching cost NN-Exp-S0 is the fastest, followed by NN-Exp-S1 and then NN-Exp-S2. The implicit NN algorithms are observed to be less accurate than the explicit ones. For example, NN-Imp-S1 is the least accurate among these algorithms, with error levels several orders

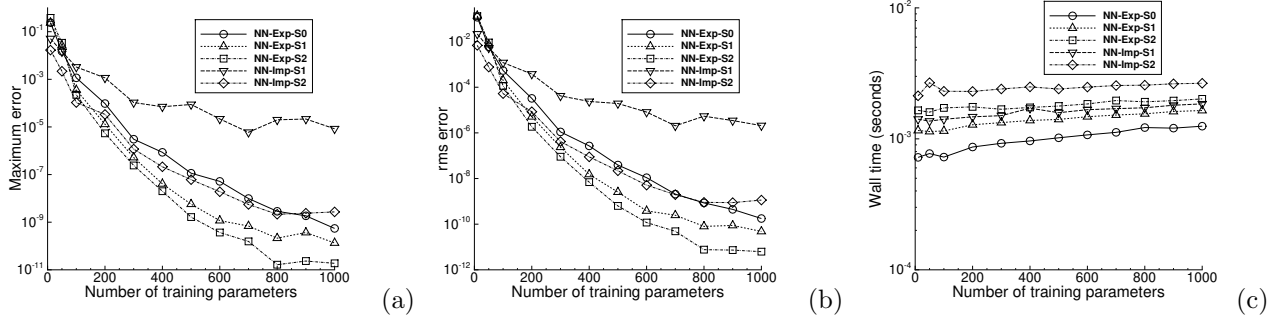


Figure 5: Linear model ($\lambda = 100$): Comparison of (a) the maximum and (b) the rms time-marching errors, and (c) the time-marching cost (wall time) versus the number of training parameters (M) among the explicit and implicit NN algorithms. $h_{\max} = 0.03$, and M is varied in the tests. NN-Exp-S0: $R_m = 0.06$, $Q = 2500$; NN-Exp-S1: $R_m = 0.5$, $Q = 2500$; NN-Exp-S2: $R_m = 0.6$, $Q = 3500$; NN-Imp-S1: $R_m = 0.5$, $Q = 2500$; NN-Imp-S2: $R_m = 0.5$, $Q = 3500$. Other simulation parameters are given in Table 2.

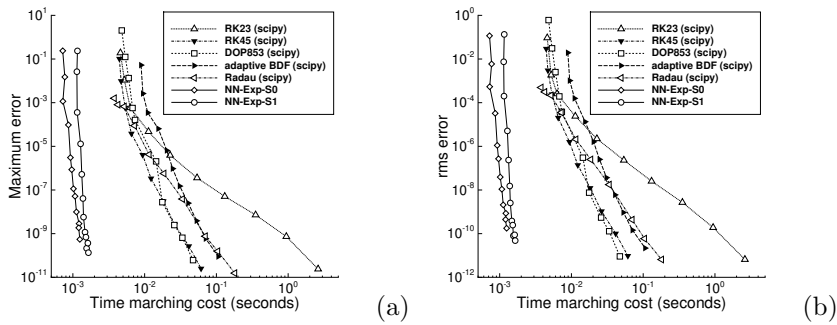


Figure 6: Linear model ($\lambda = 100$): Comparison of (a) the maximum and (b) the rms time-marching errors versus the time-marching cost (wall time) between the current NN algorithms (NN-Exp-S0 and NN-Exp-S1) and the scipy methods. The settings and parameters for NN-Exp-S0 and NN-Exp-S1 follow those of Figure 5, with data points corresponding to different M in the NN architecture. Scipy methods: adaptive time step, adaptive order, absolute tolerance 10^{-16} , data points corresponding to different relative tolerance values, dense output on points corresponding to $\Delta t = 0.02$ for $t \in [0, 1]$.

of magnitude larger than those of the other algorithms, and NN-Imp-S2 exhibits an accuracy comparable to NN-Exp-S0 for this problem. The time marching cost of the implicit NN algorithms is notably higher than that of the explicit ones. Since this test problem is linear, here the implicit NN algorithms do not actually entail the solution of nonlinear algebraic equations during time marching. For nonlinear problems in subsequent subsections the implicit NN algorithms would be considerably slower compared with the explicit ones, due to the need for solving nonlinear algebraic systems during time integration. Overall the implicit NN algorithms are not as competitive as the explicit ones.

Figure 6 shows a comparison of the computational performance (accuracy versus cost) between the NN algorithms and the traditional time integration algorithms from the scipy library. It depicts the maximum and rms time-marching errors as a function of the time-marching cost (wall time) obtained by the current NN-Exp-S0 and NN-Exp-S1 algorithms and several scipy methods, including “RK23” (explicit Runge-Kutta method of order 3(2)) [4], “RK45” (explicit Runge-Kutta method of order 5(4)) [25], “DOP853” (explicit Runge-Kutta method of order 8) [37], “Radau” (implicit Runge-Kutta method of Radau IIA family of order 5) [38], and “BDF” (implicit multi-step variable-order (orders 1 to 5) based on backward differentiation formulas enhanced with NDF modification) [5, 69]. The data for NN-Exp-S0 and NN-Exp-S1 correspond to those in Figure 5. The scipy results are obtained by employing the routine “scipy.integrate.solve_ivp()” from the scipy library with different methods. Different data points for the scipy methods correspond to

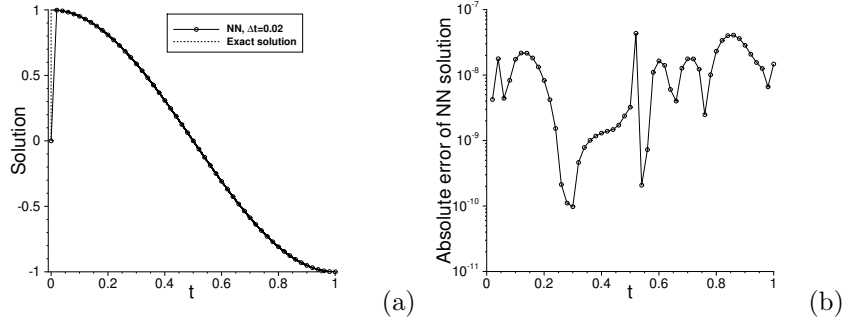


Figure 7: Linear model ($\lambda = 10^6$, stiff): (a) Comparison between the NN-Exp-S0 solution and the exact solution. (b) Absolute-error history of the NN-Exp-S0 solution. $h_{\max} = 0.025$, 2 uniform sub-domains along t_0 with enlargement factor $r = 0.05$; $M = 1000$, $Q = 1000$, $R_m = 0.4$, and $\delta_m = 0.02$. See Table 2 for the other parameter values.

different relative tolerance values, while the absolute tolerance is fixed at 10^{-16} . Since the scipy methods are adaptive in time step and order, we have used the dense output option to attain their solutions on points corresponding to a time step size $\Delta t = 0.02$ for $t \in [0, 1]$ to compute the errors. Among the scipy methods, DOP853 and RK45 show the best performance, followed by Radau and BDF, and then by RK23. The NN-Exp-S0 algorithm appears to perform slightly better than NN-Exp-S1 for this problem. Both NN-Exp-S0 and NN-Exp-S1 significantly outperform the scipy methods. Here by “outperform” we refer to the ability to achieve superior accuracy under the same time-marching cost or achieve the same accuracy under a lower time-marching cost.

We next consider a stiff case, with $\lambda = 10^6$ in problem (48). Among the explicit NN algorithms in (13)-(14), we observe that NN-Exp-S0 works well for the stiff problem, while NN-Exp-S1 works not as well as NN-Exp-S0 and NN-Exp-S2 fails to work (NN training fails to converge, with large loss values). The implicit NN algorithms from (24) also work well for this stiff problem, but is not as competitive as the explicit NN-Exp-S0 algorithm in performance.

Figure 7 illustrates the characteristics of the NN-Exp-S0 solution for this stiff case. Figure 7(a) compares the NN-Exp-S0 solution with the exact solution, and Figure 7(b) shows the absolute error of the NN-Exp-S0 solution. The training domain, the NN structure, and the other parameter values are provided in the figure caption or in Table 2. In particular, two uniform sub-domains are employed along the t_0 direction, with an enlargement factor $r = 0.05$ for network training (see Remark 2.8), and we have employed a ξ -domain map factor $\delta_m = 0.02$ when normalizing the input data on each sub-domain (see discussions at the beginning of Section 3). A time step size $\Delta t = 0.02$ is used in time marching for $t \in [0, 1]$. The NN-Exp-S0 method is highly accurate, with a maximum error on the order of 10^{-8} over the domain.

In Figure 8 we compare the maximum and rms solution errors versus the time-marching cost (wall time) obtained by the NN algorithms (NN-Exp-S0 and NN-Imp-S1) and the scipy methods for this stiff problem. The parameter values employed in these tests are provided in the figure caption or in Table 2. The explicit scipy methods (DOP853, RK45, and RK23) are not competitive for this stiff problem, as expected, inducing a large time marching cost. In contrast, the implicit scipy methods (Radau and BDF) perform considerably better. The NN-Exp-S0 algorithm is more competitive than NN-Imp-S1, but appears slightly less accurate than the latter for this problem. Both NN-Exp-S0 and NN-Imp-S1 significantly outperform the implicit and explicit scipy methods for this stiff problem.

3.2 Pendulum Problem

We test the learned NN algorithms using the nonlinear pendulum problem in this section. We study an autonomous system (free pendulum) first, followed by a non-autonomous system (forced pendulum).

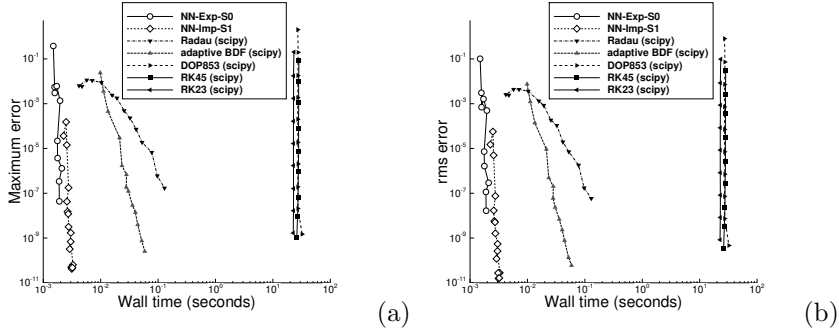


Figure 8: Linear model ($\lambda = 10^6$, stiff): Comparison of (a) the maximum and (b) the rms time-marching errors versus the time-marching cost (wall time) between the NN algorithms (NN-Exp-S0, NN-Imp-S1) and the scipy methods. NN-Exp-S0: $h_{\max} = 0.025$, $Q = 1000$, $R_m = 0.4$, $\delta_m = 0.02$; NN-Imp-S1: $h_{\max} = 0.024$, $Q = 900$, $R_m = 0.35$, $\delta_m = 0.01$; The other parameter values are provided in Table 2. Scipy methods: absolute tolerance 10^{-16} , data points corresponding to different relative tolerance values, dense output on points corresponding to $\Delta t = 0.02$ for $t \in [0, 1]$.

domain: $(y_{01}, y_{02}, \xi) \in [-2, 2] \times [-4, 4] \times [0, 0.25]$	sub-domains: 3, along y_{01} , uniform
NN (φ -subnet) architecture: $[3, M, 2]$ (M varied)	r : 0.1
activation function: Gaussian	δ_m : 1.0
Q : 900, 1000 or 1500 (random)	R_m : to be specified
Δt : 0.2 (for time marching)	time: $t \in [0, 200]$ (for time marching)

Table 3: NN simulation parameters for the free pendulum problem (Section 3.2.1).

3.2.1 Free Pendulum Oscillation

Consider the initial value problem with the free pendulum equation,

$$\frac{dy_1}{dt} = y_2, \quad \frac{dy_2}{dt} = -\alpha y_2 - \beta \sin y_1, \quad (50a)$$

$$y_1(t_0) = y_{01}, \quad y_2(t_0) = y_{02}, \quad (50b)$$

where α and β are prescribed positive constants, $y(t) = (y_1(t), y_2(t)) \in \mathbb{R}^2$ are the unknowns to be computed, t_0 is the initial time, and $y_0 = (y_{10}, y_{20}) \in \mathbb{R}^2$ are the initial conditions. Physically $y_1(t)$ represents the pendulum angle, and $y_2(t)$ is the angular velocity. In the following tests we employ $(\alpha, \beta) = (0.1, 9.8)$, $t_0 = 0$, and the initial condition $y_0 = (y_{01}, y_{02}) = (1.0, -1.0)$, unless otherwise specified.

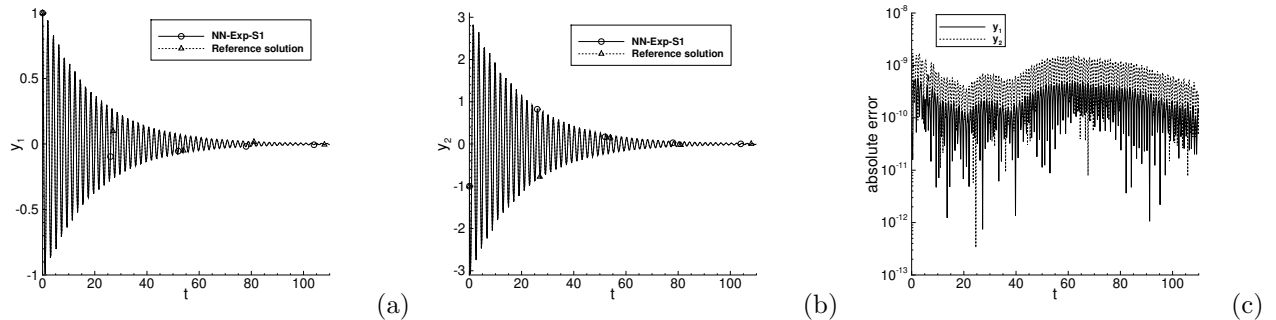


Figure 9: Free pendulum: Comparison of (a) $y_1(t)$ and (b) $y_2(t)$ between the NN-Exp-S1 solution and the reference solution. (c) Absolute-error histories of the NN-Exp-S1 solution for $y_1(t)$ and $y_2(t)$. NN-Exp-S1: $M = 800$, $Q = 1000$, $R_m = 0.6$; See Table 3 for the other parameter values.

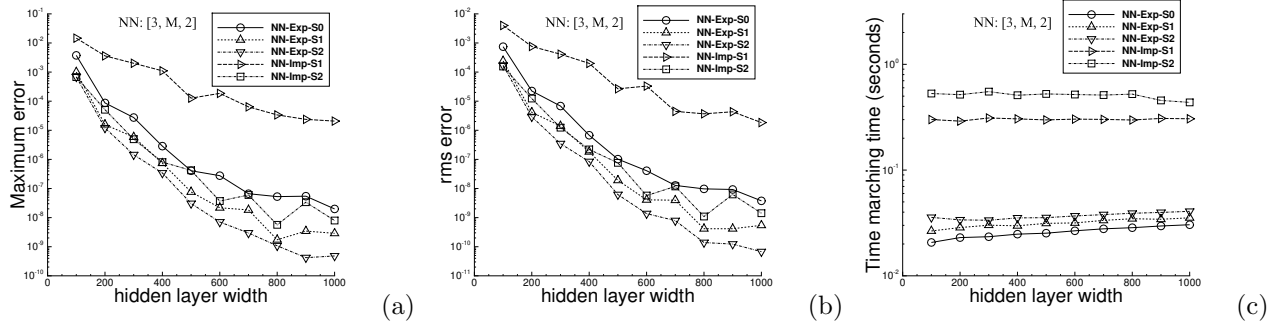


Figure 10: Free pendulum: Comparison of (a) the maximum and (b) the rms time-marching errors, and (c) the time-marching cost (wall time) versus the hidden-layer width (M) in ELM network for different NN algorithms. NN-Exp-S0: $R_m = 0.6$, $Q = 1000$. NN-Exp-S1: $R_m = 0.6$, $Q = 1000$. NN-Exp-S2: $R_m = 0.65$, $Q = 900$. NN-imp-S1: $R_m = 0.85$, $Q = 1500$. NN-imp-S2: $R_m = 0.85$, $Q = 1000$. Other parameter values are given in Table 3.

We employ an ELM network to learn the algorithmic function $\psi(y_{01}, y_{02}, \xi)$. Table 3 summarizes the simulation parameters related to the NN algorithm. In particular, we employ three uniform sub-domains along the y_{01} direction, with an enlargement factor $r = 0.1$. The parameters R_m , Δt and δ_m have the same meanings as in Section 3.1, and Q and M refer to the number of random collocation points and the hidden-layer width of the φ -subnet on each sub-domain. After the NN is trained, we employ the learned algorithm to solve the problem (50) for $t \in [0, 200]$ with a step size $\Delta t = 0.2$ and the initial condition $(y_{01}, y_{02}) = (1, -1)$. The errors of the NN solution against a reference solution and the NN time-marching time are recorded for analysis. The reference solution is obtained by the using the scipy DOP853 method with a sufficiently small tolerance (absolute tolerance 10^{-16} , relative tolerance 10^{-13}).

Figure 9 provides an overview of the solution characteristics obtained by the NN algorithm. It compares the NN-Exp-S1 solution for $y_1(t)$ and $y_2(t)$ with their reference solutions, and shows the absolute errors of the NN-Exp-S1 solutions. The parameter values are given in the figure caption or in Table 3. The NN solution is highly accurate, with a maximum error on the order of 10^{-9} for the time range.

Figure 10 is a comparison of the accuracy and the time-marching cost of different NN algorithms for solving this problem. Here we plot the maximum and rms time-marching errors (e_{\max} , e_{rms}), as well as the time-marching time, versus the hidden-layer width (M) of the φ -subnet for the NN algorithms with explicit (NN-Exp-S0, NN-Exp-S1, and NN-Exp-S2) and implicit (NN-imp-S1, and NN-imp-S2) formulations. The parameter values are listed in the figure caption or in Table 3. We can make several observations. First, the NN solution errors decrease nearly exponentially with increasing number of hidden-layer nodes, while the time-marching cost only grows quasi-linearly. Second, the explicit NN algorithms tend to be more accurate than the implicit ones. Third, among the explicit NN algorithms the accuracy generally increases from NN-Exp-S0 to NN-Exp-S1, and to NN-Exp-S2. Between the implicit NN algorithms, NN-imp-S2 is significantly more accurate than NN-imp-S1. Fourth, in terms of time-marching cost the explicit NN algorithms are much faster than the implicit ones, by an order of magnitude for this problem. Among the explicit NN algorithms, NN-Exp-S0 is the fastest, followed by NN-Exp-S1 and NN-Exp-S2. Of the implicit ones, NN-imp-S1 is notably faster than NN-imp-S2. Overall, the explicit NN algorithms are more competitive than the implicit ones. This is similar to what has been observed for the test problem in Section 3.1.

The observation that implicit NN algorithms are less competitive than the explicit ones appears to be a common characteristic in the test problems we have considered, including those in the subsequent subsections. Implicit NN algorithms are computationally much more expensive, and generally not as accurate as the explicit ones. For this reason, the computation results using the implicit NN algorithms will not be included for the simulations in the following subsections.

Figure 11 is a comparison of the computational performance (accuracy versus cost) between the NN algorithms (NN-Exp-S0 and NN-Exp-S1) and the scipy methods for the free pendulum problem. It shows the maximum and rms errors of the NN and scipy solutions versus their time-marching cost. The parameters

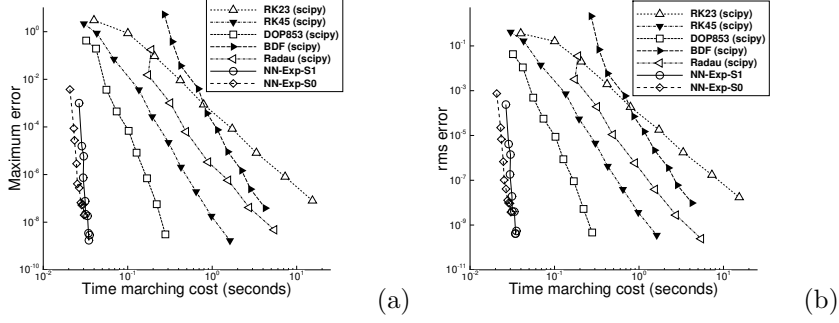


Figure 11: Free pendulum: Comparison of (a) the maximum and (b) the rms time-marching errors versus the time marching cost (wall time) between the NN algorithms (NN-Exp-S0, NN-Exp-S1) and the scipy methods. Data for the NN algorithms correspond to those of NN-Exp-S0 and NN-Exp-S1 in Figure 10. Scipy methods: absolute tolerance 10^{-16} , relative tolerance is varied, dense output on time instants corresponding to $\Delta t = 0.2$ for $t \in [0, 200]$.

domain: $(y_{01}, y_{02}, t_0, \xi) \in [-2, 2] \times [-4, 4] \times [0, 2.01] \times [0, 0.11]$	sub-domains: 3, along y_{01} , uniform
NN (φ -subnet) architecture: $[4, M, 2]$ (M varied)	r : 0.1
activation function: Gaussian	δ_m : 5.0 or 7.0
Q : 2000 or 1500, random	R_m : to be specified
Δt : 0.1 (for time marching)	time: $t \in [0, 200]$

Table 4: NN simulation parameters for the forced pendulum problem (Section 3.2.2).

and the settings for the NN algorithms correspond to those in Figure 10, in which the hidden-layer width of the φ -subnet is varied. The scipy solutions are obtained by varying the relative tolerance, with a fixed absolute tolerance 10^{-16} for different methods. Among the scipy methods, DOP853 shows the best performance, followed by RK45 and Radau. NN-Exp-S0 exhibits a slightly better performance than NN-Exp-S1. Both NN-Exp-S0 and NN-Exp-S1 significantly outperform the scipy methods.

Since the RHS of system (50) is periodic in y_1 with a period 2π , i.e. $f(y_1 + 2\pi, y_2, t) = f(y_1, y_2, t)$, the domain for the NN training only needs to cover one period along the y_{01} direction, in light of Theorem 2.4. This will be crucial for computing the NN solutions corresponding to large initial angular velocity (y_{02}) values, in which the pendulum angle (y_1) can assume large magnitudes. Figure 12 shows the NN-Exp-S1 solutions for two such cases, which exploit the periodicity of $f(y_1, y_2, t)$ during time-marching as discussed in Remark 2.10. These results correspond to an initial condition $(y_{01}, y_{02}) = (0, 6.5)$ at $t_0 = 0$, and the problem parameters $(\alpha, \beta) = (0.02, 9.8)$ and $(\alpha, \beta) = (0.005, 9.8)$, respectively. Because the initial angular velocity $y_{02} = 6.5$ is sufficiently large, the pendulum spins around the axis for several periods before settling down to oscillate around the equilibrium position (at an elevated angle y_1). The simulation parameters for this group of tests are specified in the figure caption. In particular, the NN is trained on the domain $(y_{01}, y_{02}, \xi) \in [-3.2, 3.2] \times [-6.7, 6.7] \times [0, 0.15]$, which is slightly larger than one period $[-\pi, \pi]$ along y_{01} . For time-marching using the learned $\psi(y_{01}, y_{02}, \xi)$, we exploit the periodicity of $f(y_1, y_2, t)$ as follows (see also Remark 2.10). Given (y_{1k}, y_{2k}, t_k) and the step size Δt , we compute $y_{1k}^* = \text{mod}(y_{1k} + \pi, 2\pi) - \pi$, $q = \lfloor \frac{y_{1k} + \pi}{2\pi} \rfloor$, and $(y_{1,k+1}, y_{2,k+1}) = \psi(y_{1k}^*, y_{2k}, \Delta t) + (2\pi q, 0)$. The results in Figure 12 confirm the effectiveness of the method described in Remark 2.10 for taking advantage of the RHS $f(y, t)$ that is periodic with respect to y , and show that the NN algorithm is accurate for this type of problems. Without exploiting this periodicity, one would need to use a domain having a large dimension along y_{01} to train the NN, which would pose significant challenges to network training for such problems.

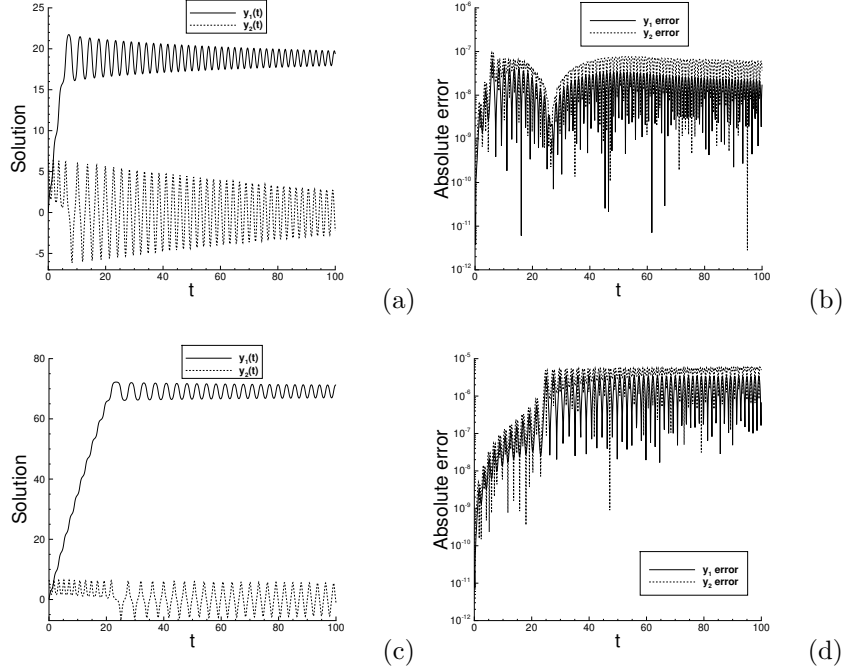


Figure 12: Free pendulum (exploiting periodicity of $f(y, t)$): NN-Exp-S1 solutions for y_1 and y_2 (left column) and their absolute errors (right column) for the problem (50) with the initial condition $(y_{01}, y_{02}) = (0, 6.5)$ and the parameters $(\alpha, \beta) = (0.02, 9.8)$ (top row) or $(\alpha, \beta) = (0.005, 9.8)$ (bottom row). Training domain: $(y_{01}, y_{02}, \xi) \in [-3.2, 3.2] \times [-6.7, 6.7] \times [0, 0.15]$, 3 uniform sub-domains along y_{01} with an enlargement factor $r = 0.1$; On each sub-domain, NN: [3, 800, 2], Gaussian activation function, $R_m = 0.6$, $Q = 1500$, $\Delta t = 0.1$ in time marching for $t \in [0, 100]$. Error computed relative to a reference solution (by scipy DOP853).

3.2.2 Forced Pendulum Oscillation

We next consider a non-autonomous system with the forced pendulum equation,

$$\frac{dy_1}{dt} = y_2, \quad \frac{dy_2}{dt} = -\alpha y_2 - \beta \sin y_1 + \gamma \cos(\pi t), \quad (51a)$$

$$y_1(t_0) = y_{01}, \quad y_2(t_0) = y_{02}, \quad (51b)$$

where γ is an additional constant and the other variables are the same as in Section 3.2.1. We employ $(\alpha, \beta, \gamma) = (0.1, 9.8, 0.2)$, $y_0 = (y_{01}, y_{02}) = (1.0, -1.0)$, and $t_0 = 0$ for this problem.

We train the NN using the parameter values from Table 4 to learn the algorithmic function $\psi(y_{01}, y_{02}, t_0, \xi)$. Since the forcing term is periodic, the RHS of (51a) satisfies $f(y_1, y_2, t + 2) = f(y_1, y_2, t)$. Therefore, we only need to learn $\psi(y_{01}, y_{02}, t_0, \xi)$ on a domain that is not smaller than 2.0 along t_0 (see Theorem 2.3). We will use $[0, 2.01]$ as the training domain along t_0 .

Figure 13 illustrates the solutions for $y_1(t)$ and $y_2(t)$, and their absolute errors, for $t \in [0, 200]$ obtained by NN-Exp-S1. The errors are computed against a reference solution attained by the scipy DOP853 method with absolute tolerance 10^{-16} and relative tolerance 10^{-13} . The reference solution is also shown in Figures 13(a,b) for comparison. The parameter values are provided in the figure caption or in Table 4. The NN solutions for $y_1(t)$ and $y_2(t)$ are highly accurate, with a maximum error on the order of 10^{-7} for a step size $\Delta t = 0.1$.

A comparison of the solution errors and the time-marching cost of different NN algorithms is provided in Figure 14. Here we plot the maximum and rms solution errors on $t \in [0, 200]$, and the time-marching time, versus the hidden-layer width M obtained by NN-Exp-S0, NN-Exp-S1 and NN-Exp-S2. The parameter values are provided in the figure caption or in Table 4. The solution errors decrease nearly exponentially with increasing M , while the time-marching cost grows only quasi-linearly as M increases. NN-Exp-S2 is more

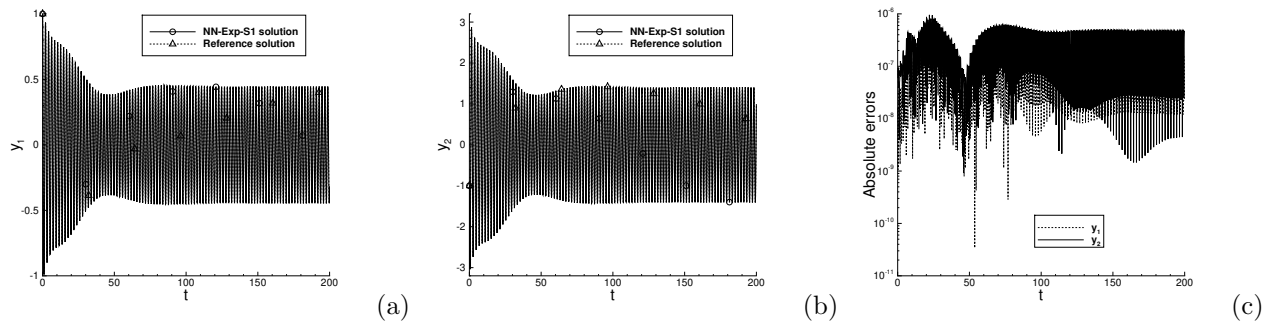


Figure 13: Forced pendulum: Comparison of (a) $y_1(t)$ and (b) $y_2(t)$ between the NN-Exp-S1 solution and the reference solution. (c) Absolute-error histories of the NN-Exp-S1 solution for $y_1(t)$ and $y_2(t)$. NN-Exp-S1: $M = 1200$, $Q = 2000$, $\delta_m = 5.0$, and $R_m = 0.4$; Other parameter values are given in Table 4. Reference solution: obtained by the scipy DOP853 method with relative tolerance 10^{-13} and absolute tolerance 10^{-16} .

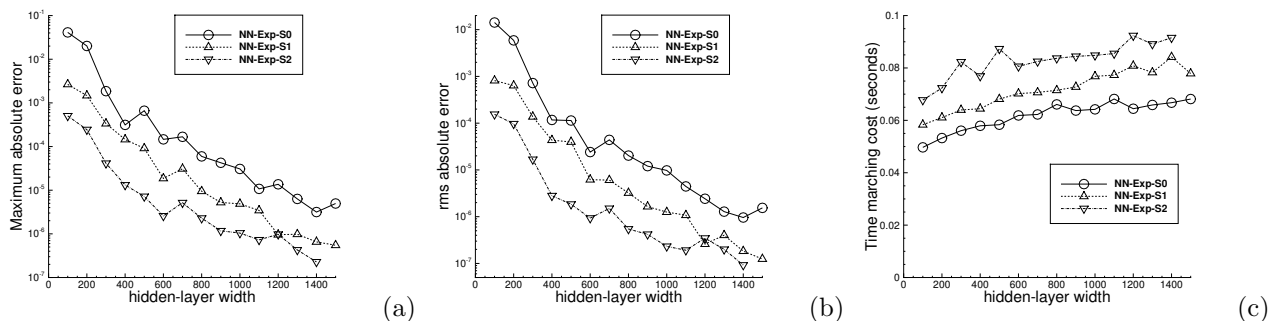


Figure 14: Forced pendulum: Comparison of (a) the maximum and (b) the rms solution errors, and (c) the time marching cost (wall time) versus the hidden-layer width M for the NN algorithms (NN-Exp-S0, NN-Exp-S1, and NN-Exp-S2). NN-Exp-S0: $Q = 2000$, $R_m = 0.3$, $\delta_m = 7.0$; NN-Exp-S1: $Q = 2000$, $R_m = 0.4$, $\delta_m = 5.0$. NN-Exp-S2: $Q = 1500$, $R_m = 0.4$, $\delta_m = 5.0$. Other parameter values are given in Table 4.

accurate than NN-Exp-S1, which in turn is more accurate than NN-Exp-S0. In terms of the time-marching cost, NN-Exp-S2 is the most expensive and NN-Exp-S0 is the least expensive among them.

A comparison of the computational performance (accuracy versus cost) between the NN algorithms and the scipy methods is shown in Figure 15. Here we plot the maximum and rms solution errors as a function of the time-marching time (for $t \in [0, 200]$) obtained by the NN-Exp-S0 and NN-Exp-S1 algorithms and the scipy methods. The two NN algorithms exhibit essentially the same performance. Among the scipy methods, DOP853 shows the best performance, followed by RK45 and the other methods. Both NN-Exp-S0 and NN-Exp-S1 markedly outperform DOP853 and the other scipy methods.

3.3 Van der Pol Oscillator

In this test we evaluate the learned NN algorithms using the van der Pol oscillator problem:

$$\frac{dy_1}{dt} = y_2, \quad \frac{dy_2}{dt} = \mu(1 - y_1^2)y_2 - y_1, \quad (52a)$$

$$y_1(t_0) = y_{01}, \quad y_2(t_0) = y_{02}, \quad (52b)$$

where $y(t) = (y_1(t), y_2(t))$ are the unknowns, $\mu > 0$ is a constant parameter, t_0 is the initial time, and $y_0 = (y_{01}, y_{02})$ are the initial data. We employ $t_0 = 0$ and $(y_{01}, y_{02}) = (2, 0)$ for time integration. This problem becomes stiff when μ is large. We use $\mu = 5$ for a non-stiff case and $\mu = 100$ for a stiff case to test the performance of the learned NN algorithms.

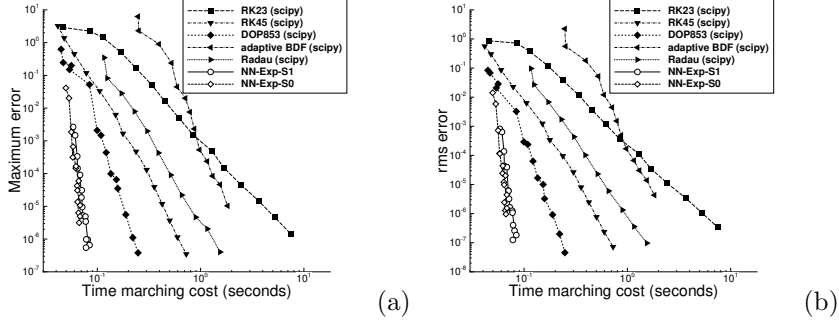


Figure 15: Forced pendulum: Comparison of (a) the maximum and (b) the rms solution errors versus the time-marching cost (wall time) between the NN algorithms (NN-Exp-S0 and NN-Exp-S1) and the scipy methods. Data for NN-Exp-S0 and NN-Exp-S1 correspond to those from Figure 14. Scipy methods: absolute tolerance 10^{-16} , data points corresponding to different relative tolerance values, dense output on points corresponding to $\Delta t = 0.1$ for $t \in [0, 200]$.

$\mu = 5$	domain: $(y_{01}, y_{02}, \xi) \in [-2.05, 2.05] \times [-8, 8] \times [0, 0.035]$ sub-domains: 3, along y_{01} , uniform r : 0.1 Q : 1500, random Δt : 0.03 (time-marching)	NN (φ -subnet): $[3, M, 2]$ activation function: Gaussian δ_m : 1 R_m : to be specified time: $t \in [0, 120]$
$\mu = 100$	domain: $(y_{01}, y_{02}, \xi) \in [-2.05, 2.05] \times [-140, 140] \times [0, h_{\max}]$ sub-domains: 3 or 5 along y_{01} (uniform); 5 along y_{02} (non-uniform), sub-domain boundaries: $[-140, -0.5, -0.03, 0.03, 0.5, 140]$ h_{\max} varied for different sub-domains r : 0.1 along y_{01} and 0.05 along y_{02} , or $r = 0$ in y_{01} and y_{02} Q : 1000 or 1400, random	NN (φ -subnet): $[3, M, 2]$ activation function: Gaussian δ_m : 1 R_m : to be specified Δt : quasi-adaptive time: $t \in [0, 300]$

Table 5: NN simulation parameters for the van der Pol oscillator (Section 3.3).

Let's first consider the problem (52) with $\mu = 5$. The simulation parameters related to the NN algorithm are listed in Table 5. In particular, we partition the training domain into uniform sub-domains along the y_{01} direction, and employ an ELM network with architecture $[3, M, 2]$ and the Gaussian activation function for the φ -subnet to learn $\psi(y_{01}, y_{02}, \xi)$, where the hidden-layer width M is varied. In this table R_m again denotes the scope of random hidden-layer coefficients.

Figure 16 illustrates characteristics of the NN solutions and their accuracy by comparing the $y_1(t)$ and $y_2(t)$ obtained by NN-Exp-S1 and a reference solution computed using the scipy DOP853 method with a sufficiently small tolerance. The absolute errors for $y_1(t)$ and $y_2(t)$ are also shown. The parameter values for these results are either specified in the caption or listed in Table 5. The NN-Exp-S1 solution is observed to be highly accurate, with a maximum error on the order of 10^{-7} for $t \in [0, 120]$.

The convergence behavior of the NN algorithms is exemplified by Figure 17. Here we plot the maximum and rms time-marching errors, as well as the time-marching cost, of NN-Exp-S0, NN-Exp-S1 and NN-Exp-S2 for $t \in [0, 120]$ as a function of the hidden-layer width M in the φ -subnet architecture. The figure caption and Table 5 provide all the parameter values corresponding to these results. It is evident that the NN solution errors decrease nearly exponentially with increasing M (before saturation), and that the time-marching cost grows only quasi-linearly as M increases.

A performance comparison (accuracy vs. cost) between the current NN algorithms and the scipy methods is provided in Figure 18. Here we plot the maximum and rms time-marching errors (for $t \in [0, 120]$) as a function of the time-marching time obtained by NN-Exp-S0 and NN-Exp-S1, and by the scipy methods. The data for NN-Exp-S0 and NN-Exp-S1 correspond to those in Figure 17, while those for the scipy methods are attained by varying the relative tolerance values. The performance of NN-Exp-S0 and NN-Exp-S1 is close,

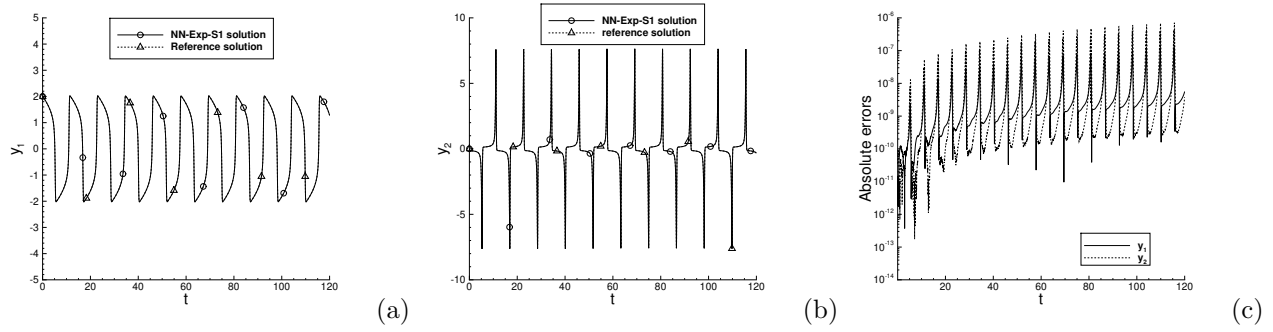


Figure 16: Van der Pol oscillator ($\mu = 5$): Comparison of (a) $y_1(t)$ and (b) $y_2(t)$ between the NN-Exp-S1 solution and the reference solution. (c) Absolute-error histories of the NN-Exp-S1 solution for $y_1(t)$ and $y_2(t)$. NN-Exp-S1: $M = 1100$, $Q = 1500$, $R_m = 0.5$; Other parameter values are given in Table 5. Reference solution: obtained by the scipy DOP853 method with absolute tolerance 10^{-16} and relative tolerance 10^{-13} .

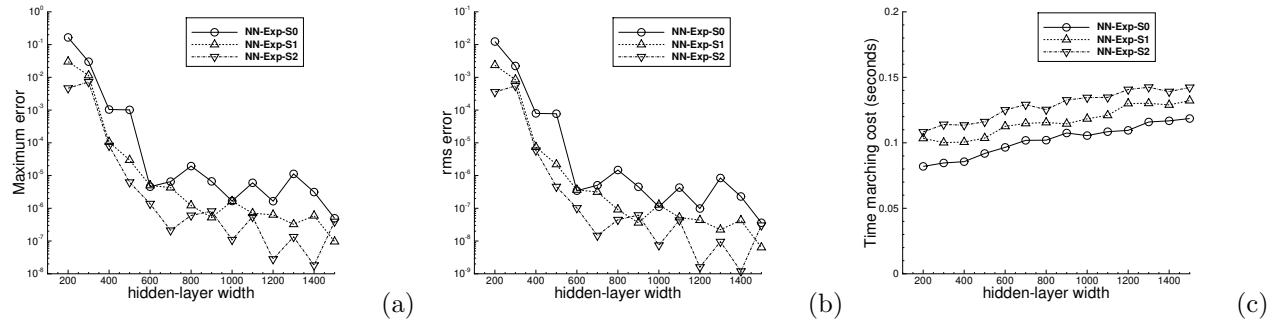


Figure 17: Van der pol oscillator ($\mu = 5$): Comparison of (a) the maximum and (b) the rms time-marching errors, and (c) the time-marching cost (wall time) versus the hidden-layer width M for the NN algorithms (NN-Exp-S0, NN-Exp-S1, NN-Exp-S2). NN-Exp-S0: $R_m = 0.45$; NN-Exp-S1: $R_m = 0.5$; NN-Exp-S2: $R_m = 0.55$. See Table 5 for the other parameter values.

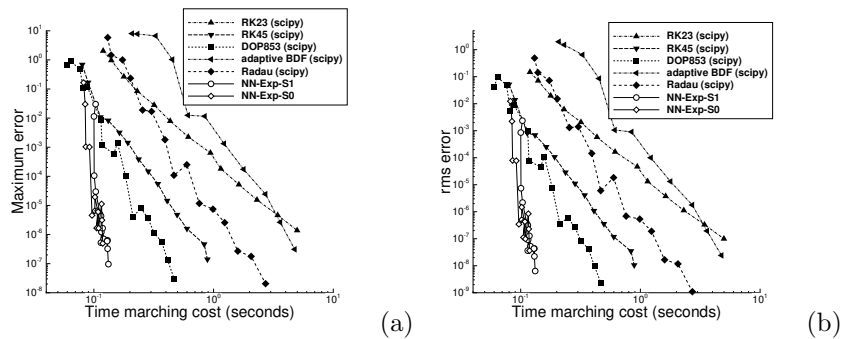


Figure 18: Van der Pol oscillator ($\mu = 5$): Comparison of (a) the maximum error and (b) the rms error versus the time marching cost (wall time) between the NN algorithms (NN-Exp-S0 and NN-Exp-S1) and the scipy methods. Data for the NN algorithms correspond to those of NN-Exp-S0 and NN-Exp-S1 in Figure 17. Scipy methods: absolute tolerance 10^{-16} , relative tolerance varied for different data points, dense output on points corresponding to $\Delta t = 0.03$ for $t \in [0, 120]$.

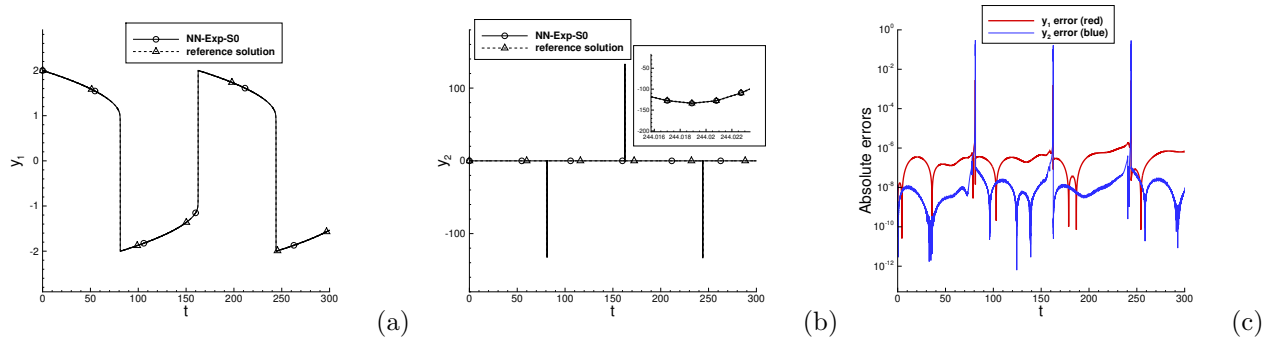


Figure 19: Van der Pol oscillator ($\mu = 100$): Comparison of (a) $y_1(t)$ and (b) $y_2(t)$ between the NN-Exp-S0 solution and the reference solution. (c) Absolute-error histories of the NN-Exp-S0 solution for $y_1(t)$ and $y_2(t)$. NN-Exp-S0: 3 uniform sub-domains in y_{01} , with enlargement factor $r = 0.1$; 5 non-uniform sub-domains in y_{02} , with enlargement factor $r = 0.05$, NN architecture: $[3, 800, 2]$ with Gaussian activation; $R_m = 0.75$, and $Q = 1400$ on each sub-domain; See Table 5 or the text for the other parameter values. Reference solution is computed by the scipy Radau method, with absolute tolerance 10^{-16} and relative tolerance 10^{-13} . The inset of plot (b) shows a magnified view around $t = 244.02$.

with the former appearing slightly better. The DOP853 method exhibits the best performance among the scipy methods, followed by RK45 and Radau. The NN-Exp-S0 and NN-Exp-S1 algorithms perform notably better than the scipy methods for this non-stiff case with the van der Pol oscillator.

We next consider the case $\mu = 100$, with which the problem (52) becomes stiff. Since the velocity of the oscillator (i.e. y_2) is very small in the majority of time but can increase to large magnitudes in bursts, using a constant step size for time integration becomes less efficient and it is necessary to incorporate some adaptive strategy into the NN algorithm.

We employ the following quasi-adaptive strategy for network training and for time integration when solving this problem. We first choose a training domain for $(y_{01}, y_{02}) \in [A_1, A_2] \times [B_1, B_2]$, and then partition this domain into m ($m \geq 1$) sub-domains along y_{01} and n ($n \geq 1$) sub-domains along y_{02} . Let $\Omega_{ij} = [a_i, a_{i+1}] \times [b_j, b_{j+1}]$ ($0 \leq i \leq m-1$, $0 \leq j \leq n-1$) denote a sub-domain, where $A_1 = a_0 < a_1 < \dots < a_m = A_2$ and $B_1 = b_0 < b_1 < \dots < b_n = B_2$. On Ω_{ij} we train a local NN to learn $\psi(y_{01}, y_{02}, \xi)$ for $(y_{01}, y_{02}, \xi) \in [a_i, a_{i+1}] \times [b_j, b_{j+1}] \times [0, h_{\max}^{(ij)}]$, where $h_{\max}^{(ij)}$ depends on Ω_{ij} and can differ in different sub-domains. This provides the opportunity, during time marching, to vary the step size based on the current value of (y_1, y_2) . Specifically for this problem, we choose h_{\max} to depend only on j , i.e. $(y_{01}, y_{02}, \xi) \in [a_i, a_{i+1}] \times [b_j, b_{j+1}] \times [0, h_{\max}^{(j)}]$ for Ω_{ij} , and we partition the domain non-uniformly along the y_{02} direction. For time integration, given (y_{1k}, y_{2k}) at time t_k , we compute the next approximation as follows:

- (i) Determine the sub-domain Ω_{ij} such that $(y_{1k}, y_{2k}) \in \Omega_{ij}$, and let $h = 0.95h_{\max}^{(j)}$.
- (ii) Compute $y_{k+1} = (y_{1,k+1}, y_{2,k+1}) = \psi(y_{1k}, y_{2k}, h)$ and $t_{k+1} = t_k + h$.

We use a training domain $(y_{01}, y_{02}) \in [-2.05, 2.05] \times [-140, 140]$ for this stiff case, as shown in Table 5, and partition the domain into 5 non-uniform sub-domains along y_{02} , with the sub-domain boundaries given by $y_{02} = [-140, -0.5, -0.03, 0.03, 0.5, 140]$. Along the y_{01} direction we partition the domain into 3 uniform sub-domains (for NN-Exp-S0), or 5 uniform sub-domains (for NN-Exp-S1). We use

$$\mathbf{h}_{\max} = (h_{\max}^{(0)}, h_{\max}^{(1)}, \dots, h_{\max}^{(4)}) = (0.002, 0.011, 0.018, 0.011, 0.002), \quad (\text{for NN-Exp-S0});$$

$$\mathbf{h}_{\max} = (h_{\max}^{(0)}, h_{\max}^{(1)}, \dots, h_{\max}^{(4)}) = (0.002, 0.011, 0.025, 0.011, 0.002), \quad (\text{for NN-Exp-S1}).$$

The NN-Exp-S2 algorithm does not work for this stiff case (training fails to converge), and the implicit NN algorithms (NN-Imp-S1, NN-Imp-S2) are not as competitive as the explicit NN-Exp-S0 and NN-Exp-S1 algorithms.

Figure 19 is a comparison of $y_1(t)$ and $y_2(t)$ between the NN-Exp-S0 solution and a reference solution obtained by the scipy Radau method, and the absolute errors of the NN-Exp-S0 solution. The values for the simulation parameters are provided in the figure caption or Table 5. The NN solution agrees well with the

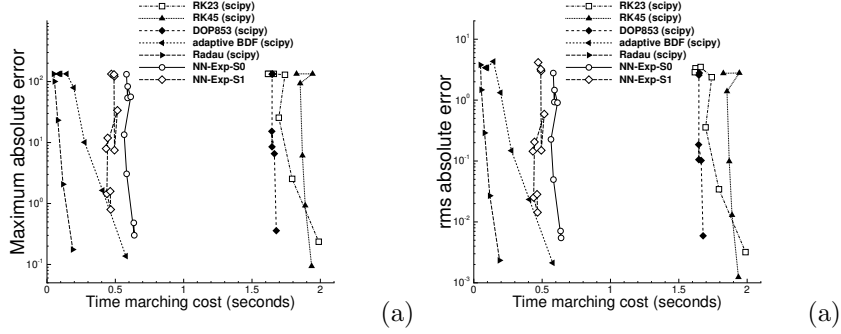


Figure 20: Van der Pol oscillator ($\mu = 100$): Comparison of (a) the maximum and (b) the rms time-marching error versus the time marching cost (wall time) between the NN algorithms (NN-Exp-S0, NN-Exp-S1) and the scipy methods for $t \in [0, 300]$. Simulation parameters for NN-Exp-S0 follow those of Figure 19. NN-Exp-S1: 5 uniform sub-domains in y_{01} with enlargement factor $r = 0$; 5 non-uniform sub-domains in y_{02} with enlargement factor $r = 0$; $R_m = 0.5$, and $Q = 1000$ on each sub-domain; See Table 5 and the text for the other parameter values. Scipy methods: absolute tolerance 10^{-16} , data points corresponding to different relative tolerance values. Errors are computed with respect to a reference solution obtained by the scipy Radau method with absolute tolerance 10^{-16} and relative tolerance 10^{-13} .

domain: $(y_{01}, y_{02}, y_{03}, \xi) \in [-20, 20] \times [-25, 25] \times [2, 46] \times [0, 0.012]$, or $(y_{01}, y_{02}, y_{03}, \xi) \in [-20, 15] \times [-27, 16] \times [2, 46] \times [0, 0.012]$	NN (φ -subnet): $[4, M, 3]$
domain decomposition: none	activation function: Gaussian
r : 0.0	δ_m : 0.2
Q : 1000 or 1200, random	R_m : to be specified
Δt : 0.01 (time-marching)	time: $t \in [0, t_f]$, $t_f = 200, 17$

Table 6: NN simulation parameters for the Lorenz63 model (Section 3.4).

reference solution, with the maximum absolute error on the order of 10^{-3} for y_1 and 10^{-1} for y_2 . The inset of Figure 19(b) shows that even at the bursts the NN method has captured the solution accurately.

Figure 20 compares the computational performance (accuracy versus cost) of the current NN algorithms and the scipy methods for this stiff case. It shows the maximum and the rms time-integration errors (e_{\max} and e_{rms}) on $t \in [0, 300]$ as a function of the time-marching time for the NN-Exp-S0 and NN-Exp-S1 algorithms and the scipy methods. The parameter values for the NN algorithms are provided in the figure caption or in Table 5. The scipy Radau method shows the best performance, followed by the scipy BDF method. The NN-Exp-S0 and NN-Exp-S1 algorithms are less competitive than the scipy Radau and BDF methods for this case. The performance of the explicit scipy methods (DOP853, RK45, and RK23) is significantly worse than the Radau/BDF and the NN-Exp-S0/NN-Exp-S1 algorithms.

3.4 Lorenz63 Chaotic System

In this subsection we test the NN algorithms using the Lorenz63 chaos model,

$$\frac{dy_1}{dt} = \sigma(y_2 - y_1), \quad \frac{dy_2}{dt} = y_1(\rho - y_3) - y_2, \quad \frac{dy_3}{dt} = y_1 y_2 - \beta y_3, \quad (53a)$$

$$y_1(t_0) = y_{01}, \quad y_2(t_0) = y_{02}, \quad y_3(t_0) = y_{03}, \quad (53b)$$

where $y(t) = (y_1(t), y_2(t), y_3(t))$ are the unknowns, $\sigma = 10$, $\rho = 28$, $\beta = 8/3$, and we employ the initial conditions $y_0 = (y_{01}, y_{02}, y_{03}) = (-10, -10, 25)$ with $t_0 = 0$ for time integration.

We learn the algorithmic function $\psi(y_{01}, y_{02}, y_{03}, \xi)$ using ELM with an architecture $[4, M, 3]$ and Gaussian activation function for the φ -subnet, where M is varied. Table 6 provides values of the simulation parameters related to the NN algorithms. No domain decomposition is used for this problem.

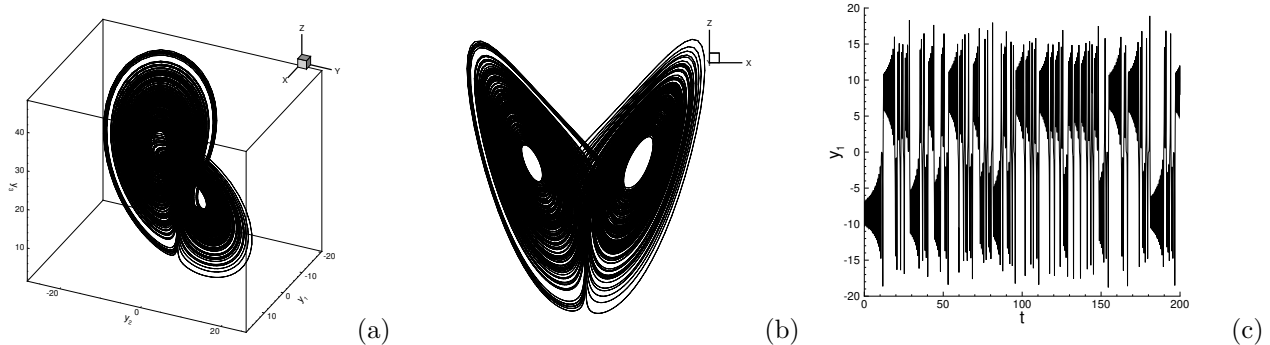


Figure 21: Lorenz63 system: (a) Perspective view, and (b) projection to the y_1 - y_3 plane of the phase space trajectories obtained by NN-Exp-S0. (c) $y_1(t)$ history. NN-Exp-S0: training domain $(y_{01}, y_{02}, y_{03}, \xi) \in [-20, 20] \times [-25, 25] \times [2, 46] \times [0, 0.012]$, NN: $[4, 900, 3]$, $Q = 1200$, $R_m = 0.12$, time integration for $t \in [0, 200]$. See Table 6 for the other parameter values.

domain: $(y_{01}, y_{02}, y_{03}, \xi) \in [-1.5, 1.8] \times [-8, 0.7] \times [2.7, 3.3] \times [0, 0.012]$, sub-domains: 4 along y_{01} (non-uniform), sub-domain boundaries: $[-1.5, -0.8, 0, 0.9, 1.8]$ r : 0.0 Q : 2000, random Δt : 0.06 (time-marching)	NN (φ -subnet): $[4, M, 3]$ activation function: Gaussian δ_m : 1 R_m : to be specified time: $t \in [0, t_f]$, $t_f = 499.8$
--	--

Table 7: NN simulation parameters for the Hindmarsh-Rose model (Section 3.5).

Figure 21 is an overview of the solution obtained by NN-Exp-S0. It shows the trajectory in phase space with two different views, as well as the time history of $y_1(t)$. The parameter values corresponding to these results are listed in the figure caption or in Table 6. The chaotic nature of the system is unmistakable.

Because the system is chaotic, comparison of different methods to compute their errors for long time integration becomes impractical. However, if the time horizon is not very long, comparing two solutions to compute the error is still physically meaningful. We next concentrate on a shorter time horizon $t \in [0, 17]$ and compare the NN algorithms with the scipy methods to evaluate their performance.

A comparison between the NN-Exp-S0 solution and a reference solution obtained by the scipy DOP853 method is provided in Figure 22. It shows the histories of y_1 , y_2 and y_3 ($t \in [0, 17]$) obtained by NN-Exp-S0 and DOP853, as well as the absolute errors between these two solutions. The parameter values corresponding to these results are provided in the caption or in Table 6. The NN solution agrees very well with the scipy solution, with the maximum error on the order of 10^{-5} in the domain.

We compare the performance (accuracy versus cost) of the learned NN algorithms and the scipy methods in Figure 23, which shows the maximum and rms time-marching errors (e_{\max} , r_{rms}) obtained by NN-Exp-S0/-S1 and the scipy methods as a function of the time-marching time on $t \in [0, 17]$. The figure caption and Table 6 provide values of the simulation parameters for these methods. The data points for NN-Exp-S0 and NN-Exp-S1 correspond to different M in the φ -subnet architecture $[4, M, 3]$, and those data points for the scipy methods correspond to different relative tolerance values. The errors are computed against a reference solution attained by the scipy DOP853 method with an absolute tolerance 10^{-16} and a relative tolerance 10^{-13} . Among the scipy methods, DOP853 exhibits the best performance, followed by RK45 and other methods. The NN-Exp-S0 and NN-Exp-S1 algorithms demonstrate a similar performance, and both notably outperform the DOP853, RK45 and the other scipy methods for this problem.

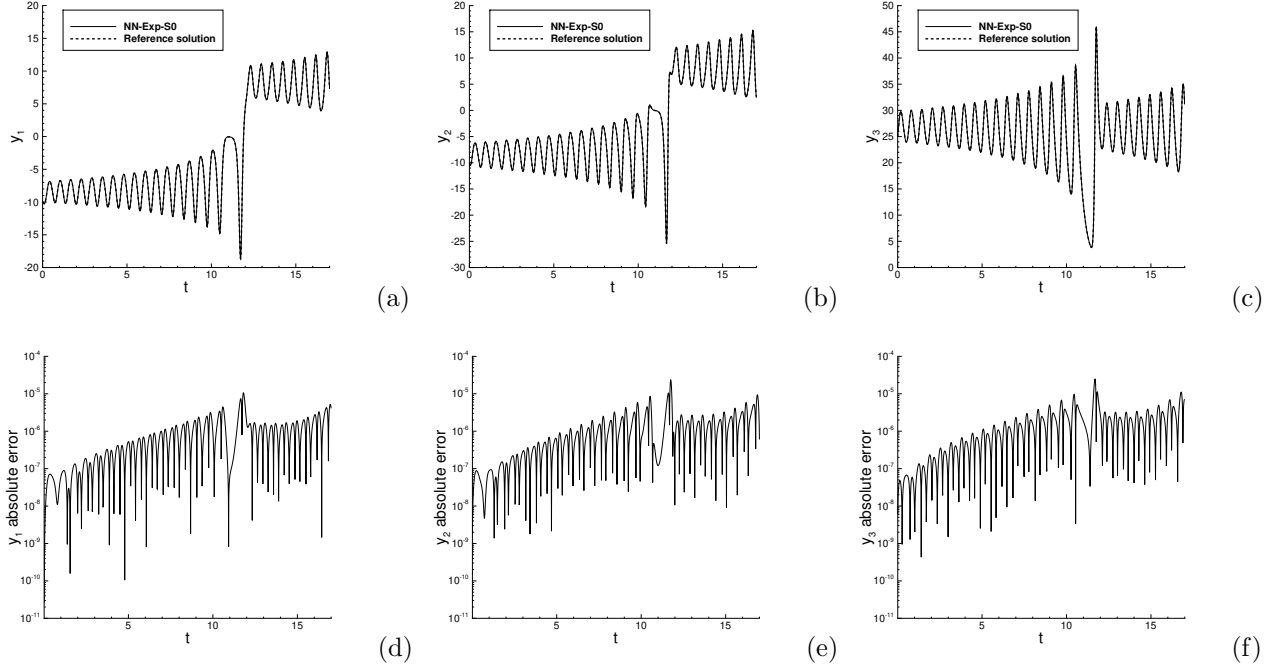


Figure 22: Lorenz63 system ($t_f = 17$): Comparison between the NN-Exp-S0 solutions and the reference solutions (top row) for y_1 , y_2 and y_3 , and the absolute errors (bottom row) of the NN-Exp-S0 solutions. Parameter values for NN-Exp-S0 follow those of Figure 21, except here for $t \in [0, 17]$. Reference solution is obtained by the scipy “DOP853” method with absolute tolerance 10^{-16} and relative tolerance 10^{-13} , with dense output on points corresponding to $\Delta t = 0.01$.

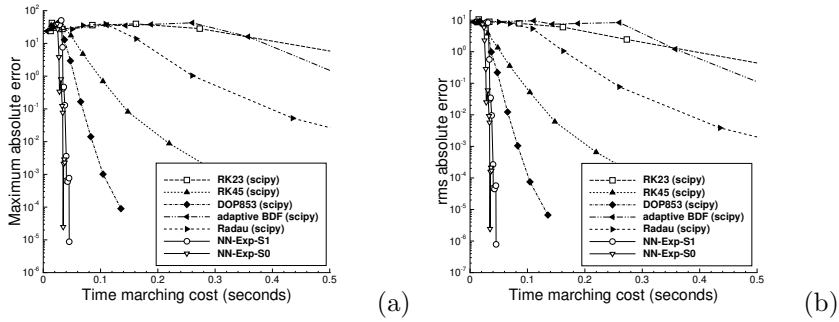


Figure 23: Lorenz63 system ($t_f = 17$): Comparison of (a) the maximum and (b) the rms solution errors versus the time marching cost (wall time) between the NN algorithms (NN-Exp-S0, NN-Exp-S1) and the scipy methods. Parameter values for NN-Exp-S0 follow those of Figure 22. NN-Exp-S1: training domain $(y_{01}, y_{02}, y_{03}, \xi) \in [-20, 15] \times [-27, 16] \times [2, 46] \times [0, 0.012]$, $R_m = 0.1$, $Q = 1000$; Other parameter values are given in Table 6. Scipy methods: absolute tolerance 10^{-16} , relative tolerance varied, dense output on points corresponding to $\Delta t = 0.01$.

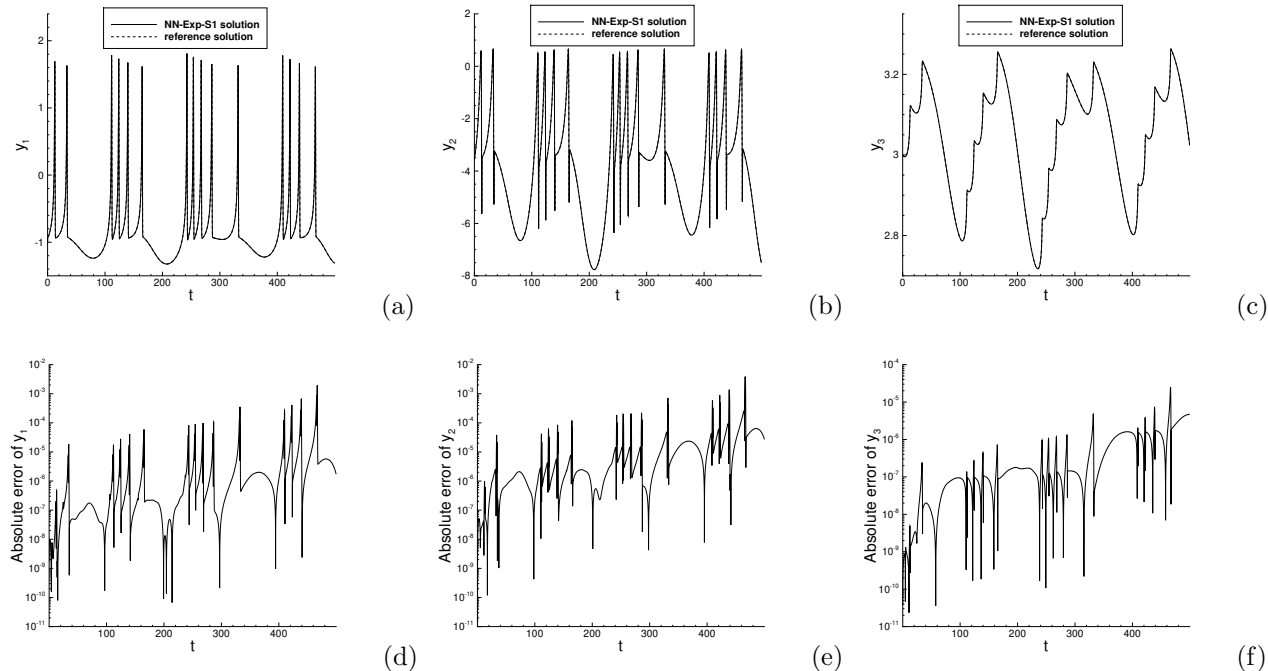


Figure 24: Hindmarsh-Rose neuron model: Comparison of (a) $y_1(t)$, (b) $y_2(t)$, and (c) $y_3(t)$ between the NN-Exp-S1 solution and the reference solution. The absolute error for (d) $y_1(t)$, (e) $y_2(t)$, and (f) $y_3(t)$ of the NN-Exp-S1 solution. NN-Exp-S1: architecture [4,1200,3] on each sub-domain, $R_m = 0.39$; Other simulation parameters are given in Table 7. Reference solution: computed by scipy DOP853, with absolute tolerance 10^{-16} and relative tolerance 10^{-13} , dense output on points corresponding to $\Delta t = 0.06$.

3.5 Hindmarsh-Rose Neuronal Model

In the next example we test the NN algorithms using the Hindmarsh-Rose model [40], which describes the spiking-bursting behavior of the membrane potential in neurons. The model is given by,

$$\frac{dy_1}{dt} = y_2 - y_1^3 + 3y_1 - y_3 + I, \quad \frac{dy_2}{dt} = 1 - 5y_1^2 - y_2, \quad \frac{dy_3}{dt} = 4\alpha \left(y_1 + \frac{8}{5} \right) - \alpha y_3, \quad (54a)$$

$$y_1(t_0) = y_{01}, \quad y_2(t_0) = y_{02}, \quad y_3(t_0) = y_{03}, \quad (54b)$$

where we employ $I = 3.1$, $\alpha = 0.006$, and the initial conditions $(y_{01}, y_{02}, y_{03}) = (-1, -3.5, 3)$ with $t_0 = 0$. Here y_1 represents the membrane potential, y_2 measures the rate of ion transport, and y_3 is an adaption current that modulates the neuron firing rate.

Table 7 lists the parameter values related to the NN algorithms for learning $\psi(y_{01}, y_{02}, y_{03}, \xi)$. In particular, we employ 4 non-uniform sub-domains along the y_{01} direction, with the sub-domain boundaries at $y_{01} = -1.5, -0.8, 0, 0.9$, and 1.8 , with an enlargement factor $r = 0$ for network training. The φ -subnet architecture is [4, M , 3] on each sub-domain, with M varied in the tests.

Figure 24 illustrates the solution characteristics for $y_1(t)$, $y_2(t)$ and $y_3(t)$ obtained by NN-Exp-S1. A reference solution for these variables obtained by the scipy DOP853 method is also shown in Figures 24(a,b,c) for comparison. The absolute errors are shown in the bottom row of the plots. The parameter values for these results are provided in the figure caption or in Table 7. The bursting behavior of the solution is evident from the history plots. The NN algorithm has captured the dynamics of the system accurately.

In Figure 25 we compare the computational performance (accuracy versus cost) between the NN algorithms and the scipy methods for the Hindmarsh-Rose model. It shows the maximum and rms time-marching errors as a function of the time-marching cost (for $t \in [0, 499.8]$) obtained by the NN-Exp-S0/NN-Exp-S1 algorithms and the scipy methods. The performance of NN-Exp-S0, NN-Exp-S1 and DOP853 is close to one

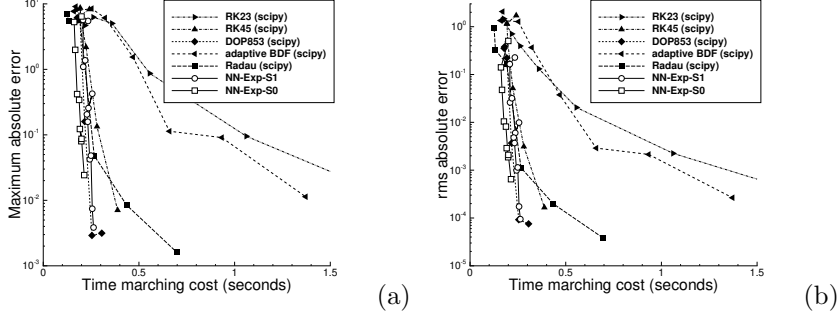


Figure 25: Hindmarsh-Rose neuron model: Comparison of (a) the maximum (b) the rms time-marching errors versus the time marching cost (wall time) between the NN algorithms (NN-Exp-S0, NN-Exp-S1) and the scipy methods. $R_m = 0.12$ for NN-Exp-S0, $R_m = 0.39$ for NN-Exp-S1; See Table 7 for the other parameter values of the NN algorithms. Scipy methods: absolute tolerance 10^{-16} , data points corresponding to different relative tolerance values.

domain: $(y_{01}, y_{02}, y_{03}, y_{04}, y_{05}, \xi) \in [-5, 10]^5 \times [0, 0.011]$, or $[-9, 12] \times [-7, 10] \times [-5.5, 11] \times [-6, 7] \times [-4, 12] \times [0, 0.011]$ sub-domains: 2 or 4 along y_{01} , uniform r : 0.0 Q : 1500 or 2000, random Δt : 0.01 (time-marching)	NN (φ -subnet): $[6, M, 5]$ activation function: Gaussian δ_m : 1 R_m : to be specified time: $t \in [0, t_f]$, $t_f = 5$ or 50
--	--

Table 8: NN simulation parameters for the Lorenz96 model (Section 3.6).

another, with NN-Exp-S0 being slightly better. These three methods show a better performance than the Radau and RK45 methods. All these methods perform significantly better than RK23 and BDF.

3.6 Lorenz96 Chaotic System

In the last example we employ the Lorenz96 chaotic system [54] to evaluate the performance of the NN algorithms. This model is given by (in 5 dimensions),

$$\frac{dy_1}{dt} = (y_2 - y_4)y_5 - y_1 + F, \quad \frac{dy_2}{dt} = (y_3 - y_5)y_1 - y_2 + F, \quad \frac{dy_3}{dt} = (y_4 - y_1)y_2 - y_3 + F, \quad (55a)$$

$$\frac{dy_4}{dt} = (y_5 - y_2)y_3 - y_4 + F, \quad \frac{dy_5}{dt} = (y_1 - y_3)y_4 - y_5 + F, \quad (55b)$$

$$y_1(t_0) = y_{01}, \quad y_2(t_0) = y_{02}, \quad y_3(t_0) = y_{03}, \quad y_4(t_0) = y_{04}, \quad y_5(t_0) = y_{05}, \quad (55c)$$

where $F = 8$, and the initial conditions are $y_0 = (y_{01}, y_{02}, y_{03}, y_{04}, y_{05}) = (-0.99, -1, -1, -1, -1)$ with $t_0 = 0$.

We learn the algorithmic function $\psi(y_{01}, y_{02}, y_{03}, y_{04}, y_{05}, \xi)$ using an ELM network with the architecture $[6, M, 5]$ and the Gaussian activation function for the φ -subnet, where M is varied. The simulation parameters for the NN algorithms are summarized in Table 8.

Figure 26 provides an overview of the solution characteristics. It shows the system trajectory ($t \in [0, 50]$) in the (y_1, y_2, y_3) phase space and the time history of y_1 obtained by the NN-Exp-S1 algorithm. The figure caption and Table 8 list the parameter values for this set of tests.

Due to the chaotic nature of the system, computing the error by comparing the solution histories in long-term evolution becomes less meaningful. We therefore consider a shorter history ($t \in [0, 5]$) and compare the current NN algorithms with the scipy methods. Figure 27 compares the solution histories for y_1, y_3 and y_4 from NN-Exp-S1 and a reference solution computed by the scipy DOP853 method (with a sufficiently small tolerance). It also shows the absolute errors for these variables from the NN-Exp-S1 solution. The NN algorithm has captured the solution accurately.

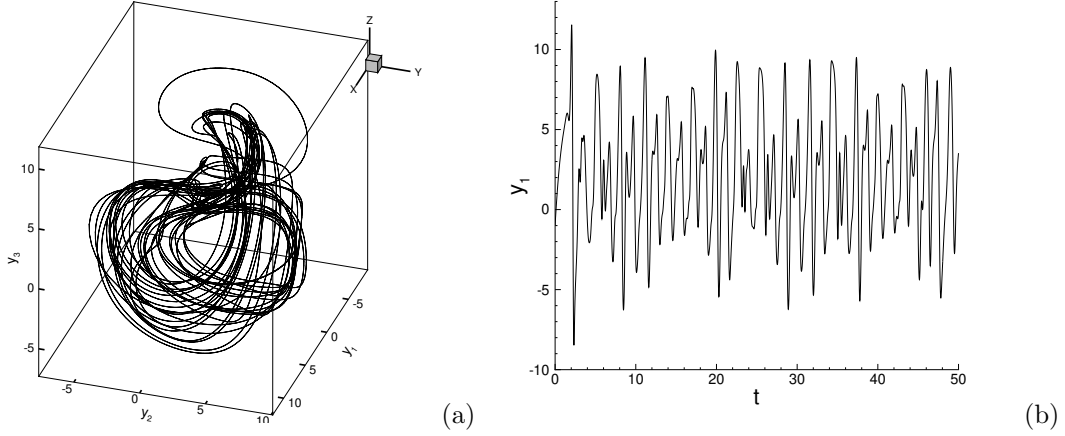


Figure 26: Lorenz96 system: (a) Trajectory in the (y_1, y_2, y_3) -phase space, and (b) the y_1 history, obtained by the NN-Exp-S1 algorithm. Training domain: $(y_{01}, y_{02}, y_{03}, y_{04}, y_{05}, \xi) \in [-5, 10]^5 \times [0, 0.011]$, with 2 uniform sub-domains along y_{01} ; NN: $[6, 800, 5]$ on each sub-domain; $R_m = 0.15$, $Q = 1500$, time integration for $t \in [0, 50]$; The Other parameter values are given in Table 8.

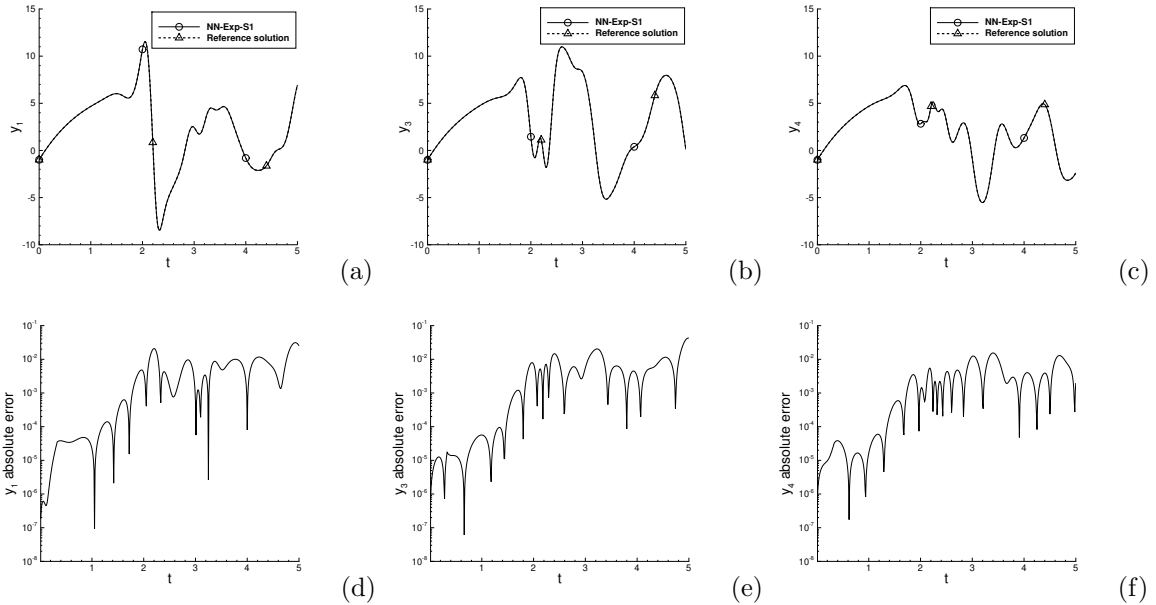


Figure 27: Lorenz96 system ($t_f = 5$): Comparison of (a) y_1 , (b) y_3 , and (c) y_4 between the NN-Exp-S1 solution and the reference solution. Absolute errors for $y_1(t)$, $y_3(t)$ and $y_4(t)$ of the NN-Exp-S1 solution. NN-Exp-S1: training domain $(y_{01}, y_{02}, y_{03}, y_{04}, y_{05}, \xi) \in [-9, 12] \times [-7, 10] \times [-5.5, 11] \times [-6, 7] \times [-4, 12] \times [0, 0.011]$, 4 uniform sub-domains along y_{01} ; NN: $[6, 1000, 5]$ on each sub-domain, $R_m = 0.15$, $Q = 1500$, time integration for $t \in [0, 5]$; See Table 8 for the other parameter values. Reference solution: obtained by scipy DOP853, with absolute tolerance 10^{-16} and relative tolerance 10^{-13} , dense output on points corresponding to $\Delta t = 0.01$.

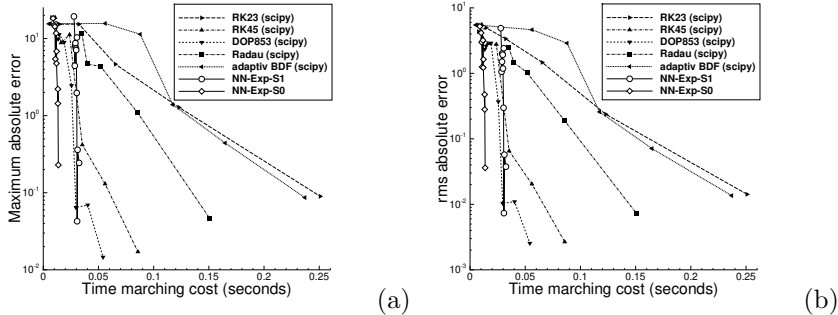


Figure 28: Lorenz96 system ($t_f = 5$): Comparison of (a) the maximum and (b) the rms time-marching errors versus the time marching cost (wall time) between the NN algorithms (NN-Exp-S0, NN-Exp-S1) and the scipy methods. NN algorithms: training domain $(y_{01}, y_{02}, y_{03}, y_{04}, y_{05}, \xi) \in [-9, 12] \times [-7, 10] \times [-5.5, 11] \times [-6, 7] \times [-4, 12] \times [0, 0.011]$, 4 uniform sub-domains along y_{01} ; NN: $[6, M, 5]$ (M varied); $R_m = 0.05$ and $Q = 2000$ for NN-Exp-S0, and $R_m = 0.15$ and $Q = 1500$ for NN-Exp-S1. See Table 8 for the other parameter values. Scipy methods: absolute tolerance 10^{-16} , data points corresponding to different relative tolerance values, dense output on points corresponding to $\Delta t = 0.01$ for $t \in [0, 5]$.

We next compare the computational performance (accuracy versus cost) between the NN algorithms and the scipy methods for the Lorenz96 system. Figure 28 shows the maximum and rms time-marching errors ($t \in [0, 5]$) as a function of the time-marching time obtained by the current NN-Exp-S0 and NN-Exp-S1 algorithms and the scipy methods. The errors are computed with respect to a reference solution obtained by the scipy DOP853 method with a sufficiently small tolerance. The parameter values for these tests are given in the figure caption or in Table 8. The data points for NN-Exp-S0 and NN-Exp-S1 correspond to different M in the φ -subnet architecture $[6, M, 5]$, while those for the scipy methods correspond to different tolerance values. Among the scipy methods DOP853 shows the best performance, followed by RK45, Radau and the other methods. The performance of NN-Exp-S1 and scipy DOP853 is close to each other. NN-Exp-S0 exhibits a better performance than NN-Exp-S1, DOP853, and the other scipy methods for this problem.

4 Concluding Remarks

We have presented a method for learning the exact time integration algorithm for non-autonomous and autonomous systems based on ELM-type randomized neural networks. The trained NN serves as a time-marching algorithm for solving the initial value problems, for arbitrary initial data or step sizes from some domain.

For a given non-autonomous (including autonomous) system, the exact time integration algorithm can be represented by an algorithmic function in higher dimensions, which satisfies an associated system of partial differential equations with corresponding boundary conditions. We learn this high-dimensional algorithmic function based on a physics informed approach, by solving the associated PDE system using ELM-type randomized NNs. We have presented several explicit and implicit formulations for the algorithmic function, which accordingly lead to explicit and implicit time integration algorithms, and discussed how to train the NN by the nonlinear least squares method. For more challenging problems, we find that it is crucial to incorporate domain decomposition into the algorithm learning. In this case the algorithmic function is represented by a collection of local randomized NNs, one for each sub-domain. Importantly, the local NNs for different sub-domains are not coupled, due to the nature of the system of equations for the algorithmic function, and thus they can be trained individually or in parallel.

Choosing the domain for the input variables for training the neural network is crucial to the accuracy of the resultant time integration algorithm and to the efficiency of network training. The training domain should be sufficiently large, in order to adequately cover the region of interest in the phase space. An overly large training domain, on the other hand, increases the difficulty in network training. When the right hand side of the non-autonomous system exhibits a periodicity with respect to any of its arguments, while the

solution itself to the problem is not periodic, we show that in this case the algorithmic function is either periodic, or when it is not, shows a well-defined relation for different periods. This property about the algorithmic function can greatly simplify the choice of the training domain and the algorithm learning.

We have performed extensive numerical experiments with benchmark problems (non-stiff, stiff, or chaotic systems) to evaluate the performance of the learned NN algorithms, and in particular to compare them with the leading traditional algorithms from the scipy library (DOP853, RK45, RK23, Radau, BDF). We have made the following observations:

- The learned NN algorithms produce highly accurate solutions with a high computational efficiency. Their solution accuracy increases nearly exponentially, while their time-marching cost grows only quasi-linearly, as the number of degrees of freedom (training collocation points, training parameters) in the ELM network increases.
- The implicit NN algorithms are not as competitive as the explicit ones, in terms of both the accuracy and the time-marching cost.
- Among the explicit NN algorithms, the accuracy increases from NN-Exp-S0 to NN-Exp-S1, and to NN-Exp-S2, under comparable simulation parameters (training data points and training parameters). The reverse is true in terms of the time-marching cost.
- The NN-Exp-S0 algorithm is observed to work well for both non-stiff and stiff problems. NN-Exp-S1 appears also able to work with both types of problems, but not as well as NN-Exp-S0 for stiff ones. On the other hand, NN-Exp-S2 encounters difficulties for stiff problems (e.g. failure to converge in NN training).
- The computational performance of the learned NN algorithms is highly competitive compared with the traditional algorithms from scipy. The NN-Exp-S0 algorithm outperforms the best of the scipy methods in most of the tests, achieving superior accuracy under a comparable time-marching cost or the same accuracy under a lower time-marching cost.

The numerical results demonstrate that the learned NN algorithms are accurate, efficient, and computationally competitive.

An outstanding problem with the learned NN algorithms is the current lack of an effective adaptive-stepping strategy, which would be crucial for efficiently solving stiff problems. The strategy described in Section 3.3 for the stiff van der Pol oscillator problem takes advantage of domain decomposition and employs different h_{\max} on different sub-domains for training the ELM network. During time integration, the time step size is adapted depending on the sub-domain that the current solution approximation falls in. This is a useful strategy, but it is only quasi-adaptive. That the NN algorithms fail to outperform the scipy Radau (or BDF) method for the stiff van der Pol oscillator case is largely due to the lack of an effective adaptive-stepping strategy. This is an important research problem and will be pursued in a future endeavor.

Acknowledgement

This work was partially supported by NSF (DMS-2012415).

Appendix: Proof of Theorems from Section 2.2.1

Proof of Lemma 2.2:

Let $z(t) = y(t + T) = y(\eta)$, where $\eta = t + T$, for $t \in \mathbb{R}$. Then

$$\frac{dz}{dt} = \frac{dy}{d\eta} = f(y(\eta), \eta) = f(z(t), t + T) = f(z, t), \quad (56)$$

where we have used equations (1) and (8). If $y(t_0) = y(t_0 + T)$, then

$$z(t_0) = y(t_0 + T) = y(t_0) = y_0. \quad (57)$$

Comparing the initial value problem consisting of (56)–(57) and the problem (1), and in light of the uniqueness under Assumption 2.1, we conclude that $z(t) = y(t)$ for all $t \in \mathbb{R}$. It follows that $y(t)$ is a periodic function with a period T .

Proof of Theorem 2.3:

Let $\Psi(y_0, t_0, \xi) = \psi(y_0, t_0 + T, \xi) = \psi(y_0, \eta, \xi)$, where $\eta = t_0 + T$, for $(y_0, t_0, \xi) \in \mathbb{R}^n \times \mathbb{R} \times [0, h_{\max}]$. Then

$$\frac{\partial \Psi}{\partial \xi} = \frac{\partial \psi}{\partial \xi} \Big|_{(y_0, \eta, \xi)} = f(\psi(y_0, \eta, \xi), \eta + \xi) = f(\Psi(y_0, t_0, \xi), t_0 + \xi + T) = f(\Psi, t_0 + \xi), \quad (58a)$$

$$\Psi(y_0, t_0, 0) = \psi(y_0, t_0 + T, 0) = y_0, \quad (58b)$$

where we have used equation (7) and the periodicity of $f(y, t)$. Comparing the problems (58) and (7), and in light of the uniqueness under Assumption 2.1, we conclude that $\Psi(y_0, t_0, \xi) = \psi(y_0, t_0, \xi)$ for all $(y_0, t_0, \xi) \in \mathbb{R}^n \times \mathbb{R} \times [0, h_{\max}]$. It follows that $\psi(y_0, t_0, \xi)$ is periodic with respect to t_0 with a period T on $(y_0, t_0, \xi) \in \mathbb{R}^n \times \mathbb{R} \times [0, h_{\max}]$.

Proof of Theorem 2.4:

Let $\Psi(y_0, t_0, \xi) = \psi(y_0 + L_i \mathbf{e}_i, t_0, \xi) = \psi(z_0, t_0, \xi)$, where $z_0 = y_0 + L_i \mathbf{e}_i \in \mathbb{R}^n$, for all $(y_0, t_0, \xi) \in \mathbb{R}^n \times \mathbb{R} \times [0, h_{\max}]$. Then

$$\frac{\partial \Psi}{\partial \xi} = \frac{\partial \psi}{\partial \xi} \Big|_{(z_0, t_0, \xi)} = f(\psi(z_0, t_0, \xi), t_0 + \xi) = f(\Psi(y_0, t_0, \xi), t_0 + \xi), \quad (59a)$$

$$\Psi(y_0, t_0, 0) = \psi(y_0 + L_i \mathbf{e}_i, t_0, 0) = y_0 + L_i \mathbf{e}_i, \quad (59b)$$

where we have used equation (7).

Let $\Phi(y_0, t_0, \xi) = \psi(y_0, t_0, \xi) + L_i \mathbf{e}_i$, for all $(y_0, t_0, \xi) \in \mathbb{R}^n \times \mathbb{R} \times [0, h_{\max}]$. Then

$$\begin{aligned} \frac{\partial \Phi}{\partial \xi} &= \frac{\partial \psi}{\partial \xi} \Big|_{(y_0, t_0, \xi)} = f(\psi(y_0, t_0, \xi), t_0 + \xi) = f(\psi(y_0, t_0, \xi) + L_i \mathbf{e}_i, t_0 + \xi) \\ &= f(\Phi(y_0, t_0, \xi), t_0 + \xi), \end{aligned} \quad (60a)$$

$$\Phi(y_0, t_0, 0) = \psi(y_0, t_0, 0) + L_i \mathbf{e}_i = y_0 + L_i \mathbf{e}_i, \quad (60b)$$

where we have used equation (7) and the periodicity condition (9) for $f(y, t)$.

Comparing the problem (59) with the problem (60), and in light of the uniqueness under Assumption 2.1, we conclude that $\Psi(y_0, t_0, \xi) = \Phi(y_0, t_0, \xi)$ for all $(y_0, t_0, \xi) \in \mathbb{R}^n \times \mathbb{R} \times [0, h_{\max}]$. This leads to equation (10).

References

- [1] P.A. Alaba, S.I. Popoola, L. Olatomiwa, M.B. Akanle, O.S. Ohunakin, E. Adetiba, O.D. Alex, A.A.A. Atayero, and W.M.A.W. Daud. Towards a more efficient and cost-sensitive extreme learning machine: a state-of-the-art review of recent trend. *Neurocomputing*, 350:70–90, 2019.
- [2] A. Bjorck. *Numerical Methods for Least Squares Problems*. SIAM, 1996.
- [3] A. Bjorck. *Numerical Methods in Matrix Computations*. Springer, 2015.
- [4] P. Bogacki and L.F. Shampine. A 3(2) pair of Runge-Kutta formulas. *Appl. Math. Lett.*, 2(4):321–325, 1989.
- [5] G.D. Byrne and A.C. Hindmarsh. A polyalgorithm for the numerical solution of ordinary differential equations. *ACM Transactions on Mathematical Software*, 1(1):71–96, 1975.
- [6] F. Calabro, S. Cuomo, D. di Serafino, G. Izzo, and E. Messina. Time discretization in the solution of parabolic pdes with anns. *Applied Mathematics and Computation*, 458:128230, 2023.
- [7] F. Calabro, G. Fabiani, and C. Siettos. Extreme learning machine collocation for the numerical solution of elliptic PDEs with sharp gradients. *Computer Methods in Applied Mechanics and Engineering*, 387:114188, 2021.
- [8] F.E. Cellier and E. Kofman. *Continuous System Simulation*. Springer, 2006.
- [9] J. Chen, X. Chi, W. E, and Z. Yang. Bridging traditional and machine learning-based algorithms for solving PDEs: the random feature method. *J. Mach. Learn.*, 1(3):268–298, 2022.
- [10] J. Chen and K. Wu. Deep-OSG: deep learning of operators in semigroup. *Journal of Computational Physics*, 493:112498, 2023.

- [11] R.T.Q. Chen, Y. Rubanova, J. Bettencourt, and D. Duvenaud. Neural ordinary differential equations. *arXiv:1806.07366*, 2019.
- [12] V. Churchill and D. Xiu. Deep learning of chaotic systems from partially-observed data. *Journal of Machine Learning for Modeling and Computing*, 3:97–119, 2022.
- [13] V. Churchill and D. Xiu. Flow map learning for unknown dynamical systems: overview, implementation, and benchmarks. *Journal of Machine Learning for Modeling and Computing*, 4:173–201, 2023.
- [14] Salvatore Cuomo, Vincenzo Schiano Di Cola, Fabio Giampaolo, Gianluigi Rozza, Maziar Raissi, and Francesco Piccialli. Scientific machine learning through physics-informed neural networks: where we are and what’s next. *J. Sci. Comput.*, 92(3):88, 2022.
- [15] S.R. de Groot and P. Mazur. *Non-Equilibrium Thermodynamics*. Dover, 1984.
- [16] M. Dellnitz, E. Hullermeier, M. Lucke, S. Ober-Blobaum, C. Offen, S. Peitz, and K. Pfannschmidt. Efficient time-stepping for numerical integration using reinforcement learning. *SIAM J. Sci. Comput.*, 45:A579–A595, 2023.
- [17] S. Dong. An efficient algorithm for incompressible N-phase flows. *Journal of Computational Physics*, 276:691–728, 2014.
- [18] S. Dong. Multiphase flows of N immiscible incompressible fluids: a reduction-consistent and thermodynamically-consistent formulation and associated algorithm. *Journal of Computational Physics*, 361:1–49, 2018.
- [19] S. Dong and Z. Li. Local extreme learning machines and domain decomposition for solving linear and nonlinear partial differential equations. *Computer Methods in Applied Mechanics and Engineering*, 387:114129, 2021. (also arXiv:2012.02895).
- [20] S. Dong and Z. Li. A modified batch intrinsic plasticity method for pre-training the random coefficients of extreme learning machines. *Journal of Computational Physics*, 445:110585, 2021. (also arXiv:2103.08042).
- [21] S. Dong and N. Ni. A method for representing periodic functions and enforcing exactly periodic boundary conditions with deep neural networks. *Journal of Computational Physics*, 435:110242, 2021.
- [22] S. Dong and Y. Wang. A method for computing inverse parametric PDE problems with random-weight neural networks. *Journal of Computational Physics*, 489:112263, 2023.
- [23] S. Dong and J. Yang. Numerical approximation of partial differential equations by a variable projection method with artificial neural networks. *Computer Methods in Applied Mechanics and Engineering*, 398:115284, 2022. (also arXiv:2201.09989).
- [24] S. Dong and J. Yang. On computing the hyperparameter of extreme learning machines: algorithms and applications to computational PDEs, and comparison with classical and high-order finite elements. *Journal of Computational Physics*, 463:111290, 2022. (also arXiv:2110.14121).
- [25] J.R. Dormand and P.J. Prince. A family of embedded Runge-Kutta formulae. *Journal of Computational and Applied Mathematics*, 6(1):19–26, 1980.
- [26] V. Dwivedi and B. Srinivasan. Physics informed extreme learning machine (pielm) – a rapid method for the numerical solution of partial differential equations. *Neurocomputing*, 391:96–118, 2020.
- [27] W. E and B. Yu. The deep Ritz method: a deep learning-based numerical algorithm for solving variational problems. *Communications in Mathematics and Statistics*, 6:1–12, 2018.
- [28] G. Fabiani, F. Calabro, L. Russo, and C. Siettos. Numerical solution and bifurcation analysis of nonlinear partial differential equations with extreme learning machines. *Journal of Scientific Computing*, 89:44, 2021.
- [29] G. Fabiani, E. Galaris, L. Russo, and C. Siettos. Parsimonious physics-informed random projection neural networks for initial value problems of ODEs and index-1 DAEs. *Chaos*, 33:043128, 2023.
- [30] G. Fabiani, I.G. Kevrekidis, C. Siettos, and A.N. Yannacopoulos. RandONets: shallow networks with random projections for learning linear and nonlinear operators. *Journal of Computational Physics*, 520:113433, 2025.
- [31] C. Flamant, P. Protopapas, and D. Sondak. Solving differential equations using neural network solution bundles. *arXiv:2006.14372*, 2020.
- [32] M. De Florio, E. Schiassi, F. Calabro, and R. Furfaro. Physics-informed neural networks for 2nd order ODEs with sharp gradients. *Journal of Computational and Applied Mathematics*, 436:115396, 2023.
- [33] C. Fronk and L. Petzold. Neural ODEs for stiff systems: implicit single-step methods. *arXiv:2410.05592*, 2024.

- [34] L. Gonon. Random feature neural networks learn Black-Scholes type PDEs without curse of dimensionality. *Journal of Machine Learning Research*, 24:1–51, 2023.
- [35] I. Goodfellow, Y. Bengio, and A. Courville. *Deep Learning*. The MIT Press, 2016.
- [36] M.E. Gurtin, E. Fried, and L. Anand. *The Mechanics and Thermodynamics of Continua*. Cambridge University Press, 2010.
- [37] E. Hairer, S.P. Norsett, and G. Wanner. *Solving Ordinary Differential Equations I*. Springer, 1993.
- [38] E. Hairer and G. Wanner. *Solving Ordinary Differential Equations II*. Springer, 1996.
- [39] A. Hamid, D. Rafiq, S.A. Nahvi, and M.A. Bazaz. Hierarchical deep learning based adaptive time stepping scheme for multiscale simulations. *arXiv:2311.05961*, 2023.
- [40] J.L. Hindmarsh and R.M. Rose. A model of neuronal bursting using three coupled first order differential equations. *Proc. R. Soc. Lond. B*, 221:87–102, 1984.
- [41] G.-B. Huang, Q.-Y. Zhu, and C.-K. Siew. Extreme learning machine: theory and applications. *Neurocomputing*, 70:489–501, 2006.
- [42] G.B. Huang, L. Chen, and C.-K. Siew. Universal approximation using incremental constructive feed-forward networks with random hidden nodes. *IEEE Transactions on Neural Networks*, 17:879–892, 2006.
- [43] B. Igel'nik and Y.H. Pao. Stochastic choice of basis functions in adaptive function approximation and the functional-link net. *IEEE Transactions on Neural Networks*, 6:1320–1329, 1995.
- [44] W. Ji, W. Qiu, Z. Shi, S. Pan, and S. Deng. Stiff-PINN: physics-informed neural networks for stiff chemical kinetics. *Journal of Physical Chemistry A*, 125:8098–8106, 2021.
- [45] G.E. Karniadakis, G. Kevrekidis, L. Lu, P. Perdikaris, S. Wang, and L. Yang. Physics-informed machine learning. *Nature Reviews Physics*, 3:422–440, 2021.
- [46] C.A. Kenedy and M.H. Carpenter. Diagonally implicit Runge-Kutta methods for ordinary differential equations. a review. *NASA/TM-2016-219173*, 2016.
- [47] S. Kim, W. Ji, S. Deng, Y. Ma, and C. Rackauckas. Stiff neural ordinary differential equations. *Chaos*, 31:093122, 2021.
- [48] A.S. Krishnapriyan, A. Gholami, S. Zhe, R.M. Kirby, and M.W. Mahoney. Characterizing possible failure modes in physics-informed neural networks. *arXiv:2109.01050*, 2021.
- [49] C. Legaard, T. Schranz, G. Schweiger, J. Drgona, B. Falay, C. Gomes, A. Iosifidis, M. Abkar, and P. Larsen. Constructing neural network based models for simulating dynamical systems. *ACM Computing Surveys*, 55:236, 2023.
- [50] S. Li, G. Liu, and S. Xiao. Extreme learning machine with kernels for solving elliptic partial differential equations. *Cognitive Computing*, 15:413–428, 2023.
- [51] H. Liu, B. Xing, Z. Wang, and L. Li. Legendre neural network method for several classes of singularly perturbed differential equations based on mapping and piecewise optimization technology. *Neural Processing Letters*, 51:2891–2913, 2020.
- [52] M. Liu, M. Hou, J. Wang, and Y. Cheng. Solving two-dimensional linear partial differential equations based on Chebyshev neural network with extreme learning machine algorithm. *Engineering Computations*, 38:874–894, 2021.
- [53] Y. Liu, J.N. Kutz, and S.L. Brunton. Hierarchical deep learning of multiscale differential equation time-steppers. *Phil. Trans. R. Soc. A*, 380:20210200, 2022.
- [54] E.N. Lorenz. Predictability: a problem partly solved. *Seminar on Predictability, ECMWF*, 1996.
- [55] H. Lu and D.M. Tartakovsky. Data-driven models of nonautonomous systems. *Journal of Computational Physics*, 507:112976, 2024.
- [56] R.E. Mickens. *Nonstandard Finite Difference Schemes*. World Scientific, 2021.
- [57] C. Moya and G. Lin. DAE-PINN: a physics-informed neural network model for simulating differential algebraic equations with application to power networks. *Neural Computing and Applications*, 35:3789–3804, 2023.
- [58] N. Ni and S. Dong. Numerical computation of partial differential equations by hidden-layer concatenated extreme learning machine. *Journal of Scientific Computing*, 95:35, 2023.
- [59] S. Panghal and M. Kumar. Optimization free neural network approach for solving ordinary and partial differential equations. *Engineering with Computers*, 37:2989–3002, 2021.
- [60] Y.H. Pao, G.H. Park, and D.J. Sobajic. Learning and generalization characteristics of the random vector functional-link net. *Neurocomputing*, 6:163–180, 1994.

- [61] M. Penwarden, A.D. Jagtap, S. Zhe, G.E. Karniadakis, and R.M. Kirby. A unified scalable framework for causal sweeping strategies for physics-informed neural networks (PINNs) and their temporal decompositions. *Journal of Computational Physics*, 493:112464, 2023.
- [62] Y. Qian, Y. Zhang, Y. Huang, and S. Dong. Physics-informed neural networks for approximating dynamic PDEs of second order in time: Error analysis and numerical algorithms. *Journal of Computational Physics*, 495:112527, 2023.
- [63] T. Qin, Z. Chen, J. Jakeman, and D. Xiu. Data-driven learning of nonautonomous systems. *SIAM J. Sci. Comput.*, 43:A1607–A1624, 2021.
- [64] T. Qin, K. Wu, and D. Xiu. Data driven governing equations approximation using deep neural networks. *Journal of Computational Physics*, 395:620–635, 2019.
- [65] H.D. Quan and H.T. Huynh. Solving partial differential equation based on extreme learning machine. *Mathematics and Computers in Simulations*, 205:697–708, 2023.
- [66] M. Raissi, P. Perdikaris, and G.E. Karniadakis. Physics-informed neural networks: a deep learning framework for solving forward and inverse problems involving nonlinear partial differential equations. *Journal of Computational Physics*, 378:686–707, 2019.
- [67] E. Schiassi, M. De Florio, B.D. Ganapol, P. Picca, and R. Furfaro. Physics-informed neural networks for the point kinetics equations for nuclear reactor dynamics. *Annals of Nuclear Energy*, 167:108833, 2022.
- [68] E. Schiassi, R. Furfaro, C. Leake, M. De Florio, H. Johnson, and D. Mortari. Extreme theory of functional connections: a fast physics-informed neural network method for solving ordinary and partial differential equations. *Neurocomputing*, 457:334–356, 2021.
- [69] L.F. Shampine and M.W. Reichelt. The matlab ODE suite. *SIAM J. Sci. Comput.*, 18(1):1–22, 1997.
- [70] J. Sirignano and K. Spoliopoulos. DGM: A deep learning algorithm for solving partial differential equations. *Journal of Computational Physics*, 375:1339–1364, 2018.
- [71] A.M. Stuart and A.R. Humphries. *Dynamical Systems and Numerical Analysis*. Cambridge University Press, 1996.
- [72] J. Sun, S. Dong, and F. Wang. Local randomized neural networks with discontinuous galerkin methods for partial differential equations. *Journal of Computational and Applied Mathematics*, 445:115830, 2024.
- [73] K. Tang, X. Wan, and Q. Liao. Adaptive deep density estimation for fokker-planck equations. *Journal of Computational Physics*, 457:111080, 2022.
- [74] X. Wan and S. Wei. VAE-KRnet and its applications to variational Bayes. *Communications in Computational Physics*, 31:1049–1082, 2022.
- [75] S. Wang and P. Perdikaris. Long-time integration of parametric evolution equations with physics-informed DeepONets. *Journal of Computational Physics*, 475:111855, 2023.
- [76] Y. Wang and S. Dong. An extreme learning machine-based method for computational PDEs in higher dimensions. *Computer Methods in Applied Mechanics and Engineering*, 418:116578, 2024.
- [77] Y. Yang, M. Hou, and J. Luo. A novel improved extreme learning machine algorithm in solving ordinary differential equations by legendre neural network methods. *Advances in Differential Equations*, 469:1–24, 2018.
- [78] Z. Yang and S. Dong. A roadmap for discretely energy-stable schemes for dissipative systems based on a generalized auxiliary variable with guaranteed positivity. *Journal of Computational Physics*, 404:109121, 2020. (also arXiv:1904.00141).
- [79] Z. Zhang, Y. Shin, and G.E. Karniadakis. GFINNs: GENERIC formalism informed neural networks for deterministic and stochastic dynamical systems. *Phil. Trans. R. Soc. A*, 380:20210207, 2022.